

A High Order Homogenization Model for Transient Dynamics of Heterogeneous Media Including Micro-Inertia Effects

Tong Hui and Caglar Oskay*

Department of Civil and Environmental Engineering
Vanderbilt University
Nashville, TN 37235

Abstract

This manuscript presents a multi-dimensional, high order homogenization model for elastic composite materials subjected to dynamic loading conditions. The proposed model is derived based on the asymptotic homogenization method with multiple spatial scales. The high order homogenization model permits implementation using the standard finite elements and shape functions since it does not involve higher order terms typically present in dispersion models. The high order homogenization model can accurately capture wave dispersion in the presence of non-uniform density and non-uniform moduli within the material microstructure. Employing the hybrid Laplace Transform/Finite Element Method, both displacement and traction boundary conditions for the macroscopic problem have been implemented. Finite element formulations for the first and second order influence functions, and the macroscale initial boundary value problem are presented. The performance of the model is verified by comparing model predictions to the local homogenization and the direct numerical simulations. The high order homogenization model is shown to predict the wave dispersion with very reasonable accuracy and cost. The proposed model can also capture the phononic bands – frequency bands within which the micro-inertia effects completely block wave propagation.

Keywords: Multiscale modeling; Computational homogenization; Composites; Wave dispersion; Homogenization

1 Introduction

This manuscript is concerned with computational modeling of wave propagation phenomena in composites and other heterogeneous materials. Composites are well known to exhibit favorable static properties such as high specific strength, specific stiffness, corrosion and fatigue resistance, and many others. These favorable properties are typically achieved by tailoring the constituent materials and the way they are put together; i.e., microstructural topology.

*Corresponding author address: VU Station B#351831, 2301 Vanderbilt Place, Nashville, TN 37235. Email: caglar.oskay@vanderbilt.edu

Composites can also be tailored to control propagation of waves and dynamic properties [24]. Depending on the wave frequencies of interest, composites with superior functional and mechanical dynamic properties ranging from radar absorption [23] to impact and blast survivability [32] have been investigated. Such favorable dynamic properties in composites can be achieved by controlling wave dispersion generated by the local motion of the microstructure (i.e., micro-inertia).

When the length of the traveling waves and the size of the material microstructure are comparable, the waveform interacts with the microstructure through reflections and refractions (i.e., dispersion) at the interfaces of constituent materials with distinct material properties (e.g., moduli and density) [27, 29]. The resulting overall dynamic response characteristics in the presence of dispersion is significantly different than those observed in an equivalent homogeneous medium characterized by homogenized moduli and density. The realization and first efforts on modeling of this phenomena dates back to the classical works of Cosserat and Cosserat [12], Mindlin [25], and Eringen and Suhubi [16] on nonlocal continuum theories.

Computational modeling of micro-inertia and dispersion is difficult because of the presence of multiple spatial scales. Three characteristic lengths are typically involved: the size of the microstructure (e.g., a unit cell or representative volume element), the length of the deformation and stress waves, and the size of the macroscopic structure or component of interest. The resolution of all microstructural features along the entire structure or component is clearly computationally prohibitive. One approach is to devise microstructure-based nonlocal effective medium theories. The effects of micro-inertia and dispersion have been recently modeled using gradient enhancement [7], time-harmonic Bloch expansions [30], scale bridging through Hamilton's principle [31], and models based on Mindlin's theory [15, 19]. These approaches require the incorporation of high order strain and inertia gradient terms to the macroscopic equations of motion.

Computational homogenization based on the mathematical homogenization theory [4, 8, 21] is another alternative for modeling wave dispersions in heterogeneous materials. In order to capture the dispersion effects, it is necessary to include higher order terms in the asymptotic expansions. Chen and Fish [11] recognized the presence of numerical instability for large time windows and proposed a space-time homogenization model that regularizes the long-time behavior in the presence of dispersion. A stable homogenization model that does not require multiple time scales was devised in [17], where higher order equilibrium terms are included in the formulation. This rigorous homogenization model is valid for microstructures with constant mass density – the dispersions are generated due to contrast in moduli of the constituents only, and only in the presence of displacement boundary conditions. Hui and Oskay [22] derived a semi-analytical dispersive model for one-dimensional problems accounting for the wave dispersion in viscoelastic composite materials. Bakhvalov and Eglit [5] applied the mathematical homogenization theory to study wave propagation in thin heterogeneous plates. Andrianov et al. [1] provided analytical solutions by incorporating the high order homogenization modeling to investigate the wave dispersion in composite rods and square lattice of

cylindrical inclusions. The two latter investigations focused on specific microstructural topologies. Recently, Fish et al. [18] proposed a new dispersion formulation, where the micro-inertia effects are introduced based on an eigenstrain formulation. This formulation was generalized to account for nonlinear behavior. Andrianov et al. [2, 3] also addressed micro-inertia effects in nonlinear heterogeneous media using the homogenization method.

In this manuscript, we develop a new high order computational homogenization model that can capture the dispersion and micro-inertia effects in composites and other heterogeneous media subjected to dynamic loading conditions. The proposed model is based on the high order computational homogenization approach introduced in Ref. [17]. In particular, this manuscript provides the following novel contributions:

1. The proposed approach leads to a numerical model that can accurately capture wave dispersion in the presence of non-uniform density, in addition to non-uniform moduli, within the material microstructure. By this approach, the full range of impedance contrast can be interrogated.
2. The hybrid Laplace Transform/Finite Element Method provides the capability to capture phononic band gaps by treating the response in the complex domain. This approach also enables the implementation of the traction boundary conditions, in addition to displacement boundary conditions.

Mathematical homogenization theory with multiple spatial scales is used to derive a higher-order homogenization model. The resulting model involves third- and fourth-order spatial derivatives and numerical implementation is not straightforward. An alternative simplified high order homogenization model without high-order spatial derivatives is introduced. The simplified high order homogenization model permits implementation using the standard finite elements and shape functions. The fourth order derivative terms are approximated using terms involving second order derivatives in time and space by exploiting asymptotic relationships, and by relating the high order moduli to the low order moduli through the use of Moore-Penrose pseudo-inverse. The performance of the high order homogenization model is assessed by comparing the model predictions to the direct numerical simulations. We note that the proposed homogenization-based model is valid when the characteristic length of the deformation and stress waves are larger (but not infinitely larger) than the size of the microstructure. When the size of the wavelengths of interest approaches to or smaller than the microstructural length scale, the wave interactions can only be captured by direct resolution of the microstructure.

Gradient elasticity models can also account for the effects of microinertia (e.g., [14, 20]). A common way to address microinertia effects is by introducing sufficient number of length scales to the gradient elasticity model. If these parameters can be properly calibrated, the gradient elasticity models can also be powerful in mimicking the microinertia effects. However, in the multidimensional setting and particularly in case of complex microstructures, the authors are not aware of clear and systematic ways of identifying these length scales. In the proposed approach, the length scale is embedded in the acceleration modulus tensor, which is numerically

computed as a function of the first and second order influence functions.

The remainder of this manuscript is organized as follows: Section 2 describes the dynamic problem of interest and the multiscale setting. Section 3 presents the formulation of the mathematical homogenization theory with multiple spatial scales and the resulting high order computational homogenization model. Section 4 provides the formulation of a simplified high order homogenization model that can be implemented using the standard finite element method. Section 5 presents the finite element formulation of the first and second order micro- and the macroscale problems for the implementation of the simplified high order homogenization method. The numerical examples to verify and assess the performance of the proposed model are discussed in Section 5. The summary, conclusions and the future research directions in this area are included in Section 6. The proof of an observation critical to the development of the simplified high order homogenization model is presented in Appendix A. Appendix B provides the properties of the Moore-Penrose pseudo-inverse, also employed in the formulation of the simplified homogenization model.

2 Problem Setting

Let $\Omega \in \mathbb{R}^{n_{sd}}$ denote the domain of a heterogeneous body subjected to dynamic loads as illustrated in Fig. 1 and n_{sd} is the number of space dimensions. The equation of motion for the body occupying Ω is:

$$\sigma_{i,j,j}^{\zeta}(\mathbf{x}, t) = \rho^{\zeta}(\mathbf{x})\ddot{u}_i^{\zeta}(\mathbf{x}, t) \quad (1)$$

where $\boldsymbol{\sigma}^{\zeta}$ denotes the stress tensor, ρ^{ζ} the density, and \mathbf{u}^{ζ} the displacement. ζ represents the dependency of response fields on microstructural heterogeneities, i.e. response fields oscillate at wavelengths of the order of characteristic volume size. \mathbf{x} denotes the position coordinate, and $t \in [0, t_0]$ the time variable, and t_0 is the end of observation period. Comma in the subscript denotes spatial derivative and overhead dot represents temporal derivative. The problem is formulated in Cartesian coordinate system using index notation following the Einstein convention (repeated indices indicate summation). Bold fonts are reserved for tensor and matrix/vector representations. The constitutive response of the heterogeneous body with elastic constituents is expressed as:

$$\sigma_{ij}^{\zeta}(\mathbf{x}, t) = C_{ijkl}^{\zeta}(\mathbf{x})\epsilon_{kl}^{\zeta}(\mathbf{x}, t) \quad (2)$$

where \mathbf{C}^{ζ} is the elastic modulus tensor, which is strongly elliptic and possesses major and minor symmetries, and $\boldsymbol{\epsilon}^{\zeta}$ the strain tensor. Under the assumption of small deformation:

$$\epsilon_{ij}^{\zeta}(\mathbf{x}, t) = \frac{1}{2} \left(u_{i,j}^{\zeta}(\mathbf{x}, t) + u_{j,i}^{\zeta}(\mathbf{x}, t) \right) \quad (3)$$

The oscillation of response fields due to microstructural heterogeneities is induced by the contrast of elastic moduli and densities of micro-constituents. Equations 1-3 are considered

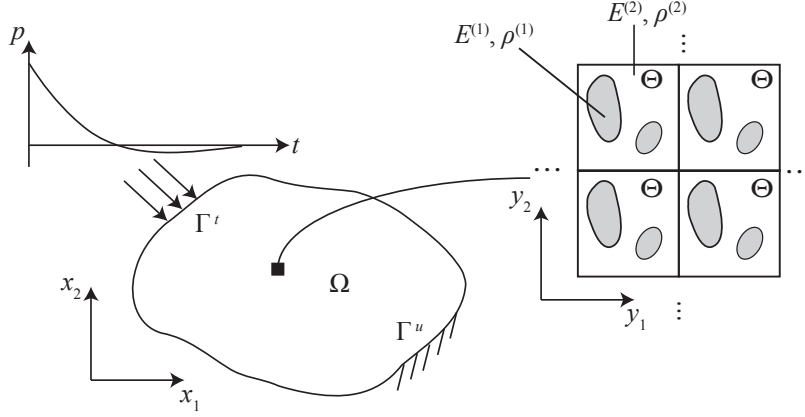


Figure 1: Schematic representation of the problem setting.

together with the following boundary conditions:

$$u_i^\zeta(\mathbf{x}, t) = \bar{u}_i(\mathbf{x}, t); \quad \mathbf{x} \in \Gamma^u \quad (4a)$$

$$\sigma_{ij}^\zeta(\mathbf{x}, t)n_j = \bar{t}_i(\mathbf{x}, t); \quad \mathbf{x} \in \Gamma^t \quad (4b)$$

in which \mathbf{n} is the outward unit normal vector along the traction boundaries. $\bar{\mathbf{u}}$ and $\bar{\mathbf{t}}$ denote the prescribed displacement and traction data on Γ^u and Γ^t , respectively. The boundary conditions are defined such that $\Gamma \equiv \partial\Omega = \Gamma^u \cup \Gamma^t$; $\Gamma^u \cap \Gamma^t = \emptyset$. The initial conditions are:

$$u_i^\zeta(\mathbf{x}, 0) = \hat{u}_i(\mathbf{x}); \quad \mathbf{x} \in \Omega \quad (5a)$$

$$\dot{u}_i^\zeta(\mathbf{x}, 0) = \hat{v}_i(\mathbf{x}); \quad \mathbf{x} \in \Omega \quad (5b)$$

where $\hat{\mathbf{u}}$ and $\hat{\mathbf{v}}$ denote the initial displacement and velocity data, respectively.

In this manuscript, the initial boundary value problem (IBVP) defined using Eqs. 1-5 is evaluated using the computational homogenization method with multiple spatial scales. The macroscale coordinate vector, \mathbf{x} , parameterizes the macroscopic domain, Ω , and the microscale (stretched) coordinate vector, \mathbf{y} , parameterizes the characteristic volume (e.g. representative volume or unit cell) denoted as Θ . \mathbf{y} is related to the macroscale coordinate system, \mathbf{x} as $\mathbf{y} = \mathbf{x}/\zeta$, where ζ is the scaling factor ($0 < \zeta < 1$) defined as the ratio between the size of the characteristic volume, Θ and the relevant shortest wavelength describing the homogenized response. An arbitrary response function, f^ζ , is expressed using the micro- and macroscopic coordinate vectors:

$$f^\zeta(\mathbf{x}) = f(\mathbf{x}, \mathbf{y}(\mathbf{x})) \quad (6)$$

The derivative of the response field is computed using the chain rule:

$$f_{,x_i}^\zeta(\mathbf{x}) = f_{,x_i}(\mathbf{x}, \mathbf{y}) + \frac{1}{\zeta} f_{,y_i}(\mathbf{x}, \mathbf{y}) \quad (7)$$

All response fields are assumed to be locally periodic over the characteristic volume throughout the deformation process:

$$f(\mathbf{x}, \mathbf{y}) = f(\mathbf{x}, \mathbf{y} + \mathbf{k}\hat{\mathbf{y}}) \quad (8)$$

where $\hat{\mathbf{y}}$ denotes the period of the microstructure; and \mathbf{k} is a $n_{\text{sd}} \times n_{\text{sd}}$ diagonal matrix with integer components.

3 Mathematical Homogenization

In this section, the multiscale representations of the response functions are used along with the asymptotic analysis of the original IBVP defined by Eqs. 1–5 to formulate a high order computational homogenization model. The displacement field is approximated using an asymptotic expansion with respect to the scaling factor, ζ :

$$u_i^\zeta(\mathbf{x}, t) = u_i(\mathbf{x}, \mathbf{y}, t) = u_i^0(\mathbf{x}, t) + \zeta u_i^1(\mathbf{x}, \mathbf{y}, t) + \zeta^2 u_i^2(\mathbf{x}, \mathbf{y}, t) + \zeta^3 u_i^3(\mathbf{x}, \mathbf{y}, t) + O(\zeta^4) \quad (9)$$

where the leading order displacement \mathbf{u}^0 is a function of macroscopic coordinate only, while the high order displacements, \mathbf{u}^α ($\alpha = 1, 2, 3 \dots$), are functions of both the macro- and microscopic coordinates. Substituting Eq. 9 to Eq. 3, the strain tensor is expressed as:

$$\epsilon_{ij}(\mathbf{x}, \mathbf{y}, t) = \epsilon_{ij}^0(\mathbf{x}, \mathbf{y}, t) + \zeta \epsilon_{ij}^1(\mathbf{x}, \mathbf{y}, t) + \zeta^2 \epsilon_{ij}^2(\mathbf{x}, \mathbf{y}, t) + O(\zeta^3) \quad (10)$$

where,

$$\epsilon_{ij}^\alpha(\mathbf{x}, \mathbf{y}, t) = e_{xij}(\mathbf{u}^\alpha) + e_{yij}(\mathbf{u}^{\alpha+1}); \quad \alpha = 0, 1, 2 \dots \quad (11)$$

$$e_{\xi ij}(\mathbf{u}^\alpha) = u_{(i, \xi_j)}^\alpha = 1/2 \left(u_{i, \xi_j}^\alpha + u_{j, \xi_i}^\alpha \right); \quad \xi = x, y \quad (12)$$

Substituting Eq. 10 into Eq. 2, the stresses are expressed as:

$$\sigma_{ij}(\mathbf{x}, \mathbf{y}, t) = \sigma_{ij}^0(\mathbf{x}, \mathbf{y}, t) + \zeta \sigma_{ij}^1(\mathbf{x}, \mathbf{y}, t) + \zeta^2 \sigma_{ij}^2(\mathbf{x}, \mathbf{y}, t) + O(\zeta^3) \quad (13)$$

where the stress components at each order of ζ are given as:

$$\sigma_{ij}^\alpha(\mathbf{x}, \mathbf{y}, t) = C_{ijkl}(\mathbf{y}) \epsilon_{kl}^\alpha(\mathbf{x}, \mathbf{y}, t); \quad \alpha = 0, 1, 2, \dots \quad (14)$$

Since microstructure is assumed to be periodic across the problem domain, the tensor of elastic moduli and the density depend on \mathbf{y} only (i.e. $\mathbf{C}^\zeta(\mathbf{x}) = \mathbf{C}(\mathbf{y})$ and $\rho^\zeta(\mathbf{x}) = \rho(\mathbf{y})$). Substituting

Eq. 13 into Eq. 1, the equations of motion at each order of ζ are obtained:

$$O(\zeta^{-1}) : \quad \sigma_{ij,y_j}^0(\mathbf{x}, \mathbf{y}, t) = 0 \quad (15a)$$

$$O(1) : \quad \sigma_{ij,x_j}^0(\mathbf{x}, \mathbf{y}, t) + \sigma_{ij,y_j}^1(\mathbf{x}, \mathbf{y}, t) = \rho(\mathbf{y})\ddot{u}_i^0(\mathbf{x}, t) \quad (15b)$$

$$O(\zeta) : \quad \sigma_{ij,x_j}^1(\mathbf{x}, \mathbf{y}, t) + \sigma_{ij,y_j}^2(\mathbf{x}, \mathbf{y}, t) = \rho(\mathbf{y})\ddot{u}_i^1(\mathbf{x}, \mathbf{y}, t) \quad (15c)$$

$$O(\zeta^2) : \quad \sigma_{ij,x_j}^2(\mathbf{x}, \mathbf{y}, t) + \sigma_{ij,y_j}^3(\mathbf{x}, \mathbf{y}, t) = \rho(\mathbf{y})\ddot{u}_i^2(\mathbf{x}, \mathbf{y}, t) \quad (15d)$$

The classical computational homogenization is based on the evaluation of the lower order equations of motion (i.e. Eqs. 15a and 15b). This practice leads to a *local* model, in which microstructural inertia effects on the system response are ignored. It is necessary to include the equations of motion at $O(\zeta)$ and $O(\zeta^2)$ to devise a computational model that captures the micro-inertia effects. We note that the inclusion of even higher order equations of motion may lead to capturing higher order dynamics induced by heterogeneous microstructures. The inclusion of additional orders also leads to increased computational cost since higher order microstructure problems need to be evaluated.

3.1 O(1) homogenization

Substituting Eqs. 11 and 14 into Eq. 15a, the balance equation at $O(\zeta^{-1})$ becomes:

$$\{C_{ijkl}(\mathbf{y}) [e_{xkl}(\mathbf{u}^0) + e_{ykl}(\mathbf{u}^1)]\}_{,y_j} = 0 \quad (16)$$

which is defined over the characteristic volume. Taking advantage of the linearity of Eq. 16 and using the separation of variables, the displacement, \mathbf{u}^1 , is expressed as:

$$u_i^1(\mathbf{x}, \mathbf{y}, t) = U_i^1(\mathbf{x}, t) + H_{ikl}(\mathbf{y})e_{xkl}(\mathbf{u}^0(\mathbf{x}, t)) \quad (17)$$

where $\mathbf{H}(\mathbf{y})$ is the first order microstructure influence function. \mathbf{H} is a 3rd rank tensor with symmetry on the second and third indices (i.e. $H_{ikl} = H_{ilk}$). Substituting Eq. 17 into Eq. 16, the equation of motion at $O(\zeta^{-1})$ is written in terms of the influence function:

$$\{C_{ijkl}(\mathbf{y})(h_{klmn}(\mathbf{y}) + I_{klmn})\}_{,y_j} = 0; \quad \mathbf{y} \in \Theta \quad (18)$$

in which $h_{ijmn}(\mathbf{y}) = H_{(i,y_j)mn}(\mathbf{y})$ is the polarization function. When furnished with appropriate boundary conditions, Eq. 18 can be solved for the first order influence function, \mathbf{H} . The local periodicity of the first order displacement field, \mathbf{u}^1 , leads to the periodicity of the first order influence function. \mathbf{H} is normalized to ensure uniqueness:

$$\langle H_{ikl}(\mathbf{y}) \rangle = \frac{1}{|\Theta|} \int_{\Theta} H_{ikl}(\mathbf{y}) d\mathbf{y} = 0 \quad (19)$$

in which $\langle \cdot \rangle = \frac{1}{|\Theta|} \int_{\Theta} \cdot d\mathbf{y}$ denotes the averaging operator, and $|\Theta|$ is the volume of Θ . Eq. 19 is necessary to ensure that the influence function problem has a unique solution. By ensuring that the average of the influence function vanishes, the rigid body modes are eliminated from the solution. The boundary value problem for \mathbf{H} is summarized in Box 1.

Given : The tensor of elastic moduli, $\mathbf{C}(\mathbf{y})$.

Find : The first order influence function, $\mathbf{H} : \Theta \rightarrow \mathbb{R}^{n_{sd} \times n_{sd} \times n_{sd}}$, such that:

- Equilibrium:

$$\{C_{ijkl}(\mathbf{y}) [h_{klmn}(\mathbf{y}) + I_{klmn}]\}_{,y_j} = 0; \quad \mathbf{y} \in \Theta$$

$$h_{ijmn}(\mathbf{y}) = 1/2 (H_{imn,y_j}(\mathbf{y}) + H_{jmn,y_i}(\mathbf{y})); \quad \mathbf{y} \in \Theta$$

- Periodicity condition at the microscale:

$$H_{ikl}(\mathbf{y}) = H_{ikl}(\mathbf{y} + \mathbf{k}\hat{\mathbf{y}}); \quad \mathbf{y} \in \Gamma_{\Theta} = \partial\Theta$$

- Normalization condition:

$$\langle H_{ikl}(\mathbf{y}) \rangle = 0; \quad \mathbf{y} \in \Theta$$

Box 1: Summary of the boundary value problem for $\mathbf{H}(\mathbf{y})$.

Applying the averaging operator to Eq. 15b and exploiting the local periodicity of $\boldsymbol{\sigma}^1$, the homogenized equation of motion at $O(1)$ is written as:

$$\rho_0 \ddot{u}_i^0(\mathbf{x}, t) = D_{ijmn}^0 e_{xmn}(\mathbf{u}^0)_{,x_j}; \quad \mathbf{x} \in \Omega \quad (20)$$

where $\rho_0 = \langle \rho \rangle$ is the volume-averaged density; and

$$D_{ijmn}^0 = \langle C_{ijmn}^0(\mathbf{y}) \rangle \quad (21)$$

$$C_{ijmn}^0(\mathbf{y}) = C_{ijkl}(\mathbf{y})(h_{klmn}(\mathbf{y}) + I_{klmn}) \quad (22)$$

in which, \mathbf{D}^0 is the zeroth homogenized elastic modulus tensor and \mathbf{I} is the fourth order identity tensor. The homogenized equation of motion at $O(1)$, along with the initial and boundary conditions, can be evaluated for \mathbf{u}^0 . The IBVP for evaluating \mathbf{u}^0 is summarized in Box 2. This model cannot account for micro-inertia effects as illustrated by the numerical examples below.

Given: The homogenized elastic modulus tensor, \mathbf{D}^0 , the volume-averaged density ρ_0 , and the initial and boundary data, $\bar{\mathbf{u}}(\mathbf{x}, t)$, $\bar{t}(\mathbf{x}, t)$, $\hat{\mathbf{u}}(\mathbf{x})$, $\hat{\mathbf{v}}(\mathbf{x})$.

Find: The macroscopic deformation, $\mathbf{u}^0 : \Theta \times [0, t_0] \rightarrow \mathbb{R}^{n_{sd}}$ such that:

- Equation of motion:

$$\rho_0 \ddot{u}_i^0(\mathbf{x}, t) = D_{ijmn}^0 e_{xmn}(\mathbf{u}^0)_{,x_j}; \quad \mathbf{x} \in \Omega$$

- Boundary conditions:

$$u_i^0(\mathbf{x}, t) = \bar{u}_i(\mathbf{x}, t); \quad \mathbf{x} \in \Gamma^u;$$

$$D_{ijmn}^0 (e_{xmn}(\mathbf{u}^0)) n_j = \bar{t}_i(\mathbf{x}, t); \quad \mathbf{x} \in \Gamma^t$$

- Initial conditions:

$$u_i^0(\mathbf{x}, 0) = \hat{u}_i(\mathbf{x}); \quad \mathbf{x} \in \Omega$$

$$\dot{u}_i^0(\mathbf{x}, 0) = \hat{v}_i(\mathbf{x}); \quad \mathbf{x} \in \Omega$$

Box 2: Summary of the initial boundary value problem for \mathbf{u}^0 .

3.2 $O(\zeta)$ homogenization

Substituting Eq. 20 to Eq. 15b and considering Eqs. 11 and 14, the equation of motion at $O(1)$ is expressed as:

$$\begin{aligned} \{C_{ijkl}(\mathbf{y}) [e_{ykl}(\mathbf{u}^2) + e_{xkl}(\mathbf{U}^1) + H_{kmn}(\mathbf{y}) e_{xmn}(\mathbf{u}^0)_{,x_l}]\}_{,y_j} \\ = \{[\theta(\mathbf{y}) D_{ijmn}^0 - C_{ijmn}^0(\mathbf{y})] e_{xmn}(\mathbf{u}^0)\}_{,x_j} \end{aligned} \quad (23)$$

where $\theta(\mathbf{y}) = \rho(\mathbf{y})/\rho_0$. The second order displacement, \mathbf{u}^2 , is approximated by introducing the second order influence function, $\mathbf{P}(\mathbf{y})$. Exploiting the linearity of Eq. 23:

$$u_i^2(\mathbf{x}, \mathbf{y}, t) = U_i^2(\mathbf{x}, t) + H_{ikl}(\mathbf{y}) e_{xkl}(\mathbf{U}^1) + P_{ijkl}(\mathbf{y}) e_{xkl}(\mathbf{u}^0)_{,x_j} \quad (24)$$

in which \mathbf{P} is a fourth rank tensor and symmetric with respect to the last two indices, but not necessarily with respect to the first two indices (i.e., $P_{ijkl} \neq P_{jikl}$ and $P_{ijkl} \neq P_{klij}$) for arbitrary microstructural configurations. Substituting Eq. 24 into Eq. 23, the equation of motion at $O(\zeta^0)$ is derived as:

$$C_{ijpmn,y_j}^1 = \theta(\mathbf{y}) D_{ipmn}^0 - C_{ipmn}^0(\mathbf{y}); \quad \mathbf{y} \in \Theta \quad (25)$$

and

$$C_{ijpmn}^1(\mathbf{y}) = C_{ijkl} \{p_{klpmn}(\mathbf{y}) + H_{kmn}(\mathbf{y}) \delta_{lp}\} \quad (26)$$

in which $p_{klpmn}(\mathbf{y}) = P_{(k,y_l)pmn}/2$ and δ is the Kronecker delta. The periodicity and the normalization conditions are employed similarly to the BVP for the first order influence function, \mathbf{H} . The summary of the boundary value problem for the second order influence function is summarized in Box 3.

Given: The material properties, \mathbf{C} and \mathbf{D}^0 , and the first order influence function, $\mathbf{H}(\mathbf{y})$.

Find: The second order influence function, $\mathbf{P}(\mathbf{y}) : \Theta \rightarrow \mathbb{R}^{n_{sd} \times n_{sd} \times n_{sd} \times n_{sd}}$ such that:

- Equilibrium:

$$C_{ijkl}(\mathbf{y}) \{p_{klpmn}(\mathbf{y}) + H_{kmn}(\mathbf{y})\delta_{lp}\}_{y_j} = \theta(\mathbf{y})D_{ipmn}^0 - C_{ipmn}^0(\mathbf{y}); \quad \mathbf{y} \in \Theta$$

$$p_{klpmn} = \frac{1}{2}(P_{kpmn,y_l} + P_{lpmn,y_k}); \quad \mathbf{y} \in \Theta$$
- Periodicity condition at the microscale:

$$P_{ijkl}(\mathbf{y}) = P_{ijkl}(\mathbf{y} + \mathbf{k}\hat{\mathbf{y}}); \quad \mathbf{y} \in \Gamma_\Theta$$
- Normalization condition:

$$\langle P_{ijkl}(\mathbf{y}) \rangle = 0; \quad \mathbf{y} \in \Theta$$

Box 3: Summary of the boundary value problem for $\mathbf{P}(\mathbf{y})$.

Substituting Eqs. 17 and 24 into Eq. 14, the first order stress tensor is expressed as:

$$\sigma_{ij}^1(\mathbf{x}, \mathbf{y}, t) = C_{ijmn}^0(\mathbf{y})e_{xmn}(\mathbf{U}^1) + C_{ijpmn}^1(\mathbf{y})e_{xmn}(\mathbf{u}^0)_{,x_p} \quad (27)$$

Applying the averaging operator to Eq. 15c, using Eq. 27 and the local periodicity of σ^2 , the homogenized equation of motion at $O(\zeta)$ takes the form:

$$\rho_0 \ddot{U}_i^1 + \langle \rho(\mathbf{y})H_{ikl}(\mathbf{y}) \rangle e_{xkl}(\ddot{\mathbf{u}}^0) = D_{ijmn}^0 e_{xmn}(\mathbf{U}^1)_{,x_j} + D_{ijkmn}^1 e_{xmn}(\mathbf{u}^0)_{,x_k x_j}; \quad \mathbf{x} \in \Omega \quad (28)$$

where the first order homogenized stiffness tensor, \mathbf{D}^1 , is defined as:

$$D_{ijpmn}^1 = \langle C_{ijpmn}^1(\mathbf{y}) \rangle \quad (29)$$

3.3 $O(\zeta^2)$ homogenization

The homogenization at $O(\zeta^2)$ follows a similar procedure to $O(\zeta)$ homogenization. Substituting Eq. 28 to Eq. 15c, and exploiting Eqs. 14, 17, 20, and 24 yield:

$$\begin{aligned} & \{C_{ijkl}(\mathbf{y}) [e_{ykl}(\mathbf{u}^3) + e_{xkl}(\mathbf{U}^2) + H_{kmn}(\mathbf{y})e_{xmn}(\mathbf{U}^1)_{,x_l} + P_{krmn}(\mathbf{y})e_{xmn}(\mathbf{u}^0)_{,x_r x_l}] \} \\ & = \{ [\theta(\mathbf{y})D_{ijlmn}^1 - C_{ijlmn}^1(\mathbf{y})] + \theta(\mathbf{y}) [H_{ikl}(\mathbf{y}) - \rho_0^{-1} \langle \rho(\mathbf{y})H_{ikl}(\mathbf{y}) \rangle] D_{kijmn}^0 \} e_{xmn}(\mathbf{u}^0)_{,x_j x_l} \\ & \quad + \{ \theta(\mathbf{y})D_{ijmn}^0 - C_{ijmn}^0(\mathbf{y}) \} e_{xmn}(\mathbf{U}^1)_{,x_j} \quad (30) \end{aligned}$$

Due to the linearity of Eq. 30, the third order displacement, \mathbf{u}^3 , is approximated by introducing the third order influence function, $\mathbf{Q}(\mathbf{y})$:

$$u_i^3(\mathbf{x}, \mathbf{y}, t) = U_i^3(\mathbf{x}, t) + H_{ikl}(\mathbf{y})e_{xkl}(\mathbf{U}^2) + P_{ijkl}(\mathbf{y})e_{xkl}(\mathbf{U}^1)_{,x_j} + Q_{ijkmn}(\mathbf{y})e_{xmn}(\mathbf{u}^0)_{,x_k x_j} \quad (31)$$

Substituting Eq. 31 to Eq. 30, the governing equation for the third order influence function, after some algebra, becomes:

$$C_{ijprmn,y_j}^2 = \theta(\mathbf{y})D_{irpmn}^1 - C_{irpmn}^1(\mathbf{y}) + \theta(\mathbf{y}) \{H_{ikp}(\mathbf{y}) - \rho_0^{-1}\langle \rho H_{ikp} \rangle\} D_{krmn}^0; \quad \mathbf{y} \in \Theta \quad (32)$$

where

$$C_{ijprmn}^2(\mathbf{y}) = C_{ijkl}(\mathbf{y}) \{q_{klprmn}(\mathbf{y}) + P_{krmn}(\mathbf{y})\delta_{lp}\} \quad (33)$$

in which $q_{klprmn} = Q_{(k,y_l)prmn}$. The third order influence function, \mathbf{Q} , is a fifth rank tensor with minor symmetry only on the last two indices (i.e. $Q_{ijkmn} = Q_{ijknm}$). Since the explicit computation of \mathbf{Q} is not necessary in the high order homogenization model described below, the BVP for \mathbf{Q} is not discussed further. Substituting Eqs. 24 and 31 to Eq. 14 yields:

$$\sigma_{ij}^2(\mathbf{x}, \mathbf{y}, t) = C_{ijmn}^0(\mathbf{y})e_{xmn}(\mathbf{U}^2) + C_{ijrnm}^1(\mathbf{y})e_{xmn}(\mathbf{U}^1)_{,x_r} + C_{ijprmn}^2(\mathbf{y})e_{xmn}(\mathbf{u}^0)_{,x_r x_p} \quad (34)$$

Applying the averaging operator to Eq. 15d, exploiting Eq. 34 and considering that σ^3 is locally periodic, the homogenized equation of motion at $O(\zeta^2)$ is then derived as:

$$\begin{aligned} \rho_0 \ddot{U}_i^2(\mathbf{x}, t) + \langle \rho(\mathbf{y})H_{ikl}(\mathbf{y}) \rangle e_{xkl}(\ddot{\mathbf{U}}^1) + \langle \rho(\mathbf{y})P_{ijkl}(\mathbf{y}) \rangle e_{xkl}(\ddot{\mathbf{u}}^0)_{,y_j} \\ = D_{ijmn}^0 e_{xmn}(\mathbf{U}^2)_{,x_j} + D_{ijrnm}^1 e_{xmn}(\mathbf{U}^1)_{,x_r x_j} + D_{ijprmn}^2 e_{xmn}(\mathbf{u}^0)_{,x_r x_p x_j}; \quad \mathbf{x} \in \Omega \end{aligned} \quad (35)$$

where the second order homogenized stiffness tensor, \mathbf{D}^2 , is expressed as:

$$D_{ijprmn}^2 = \langle C_{ijprmn}^2(\mathbf{y}) \rangle \quad (36)$$

It is possible to express the second order homogenized stiffness tensor, \mathbf{D}^2 , as a function of the first and second influence functions, eliminating the dependence on \mathbf{Q} [17]:

$$\begin{aligned} D_{ijprmn}^2 = \rho_0^{-1} \langle \rho(\mathbf{y})P_{qrmn}(\mathbf{y}) \rangle D_{pqij}^0 + \rho_0^{-1} \langle \rho(\mathbf{y})H_{sij}(\mathbf{y}) \rangle D_{srpmn}^1 \\ + \langle p_{klrnm}(\mathbf{y})C_{klpij}^1(\mathbf{y}) \rangle - \langle H_{sij}(\mathbf{y})C_{srpmn}^1(\mathbf{y}) \rangle + \rho_0^{-1} \langle \rho(\mathbf{y})H_{sij}(\mathbf{y})H_{spq}(\mathbf{y}) \rangle D_{qrmn}^0 \\ - \rho_0^2 \langle \rho(\mathbf{y})H_{sij}(\mathbf{y}) \rangle \langle \rho(\mathbf{y})H_{spq}(\mathbf{y}) \rangle D_{qrmn}^0 \end{aligned} \quad (37)$$

Considering a homogenized displacement field by including the first two orders of the displacement decomposition and averaging over the characteristic volume:

$$U_i(\mathbf{x}, t) = \langle u_i(\mathbf{x}, \mathbf{y}, t) \rangle = u_i^0 + \zeta U_i^1 + \zeta^2 U_i^2 + O(\zeta^3) \quad (38)$$

The summation of Eqs. 20, 28 and 35 leads to a high order homogenized equation of motion in terms of the mean displacement, \mathbf{U} . Neglecting $O(\zeta^3)$ and the higher order terms:

$$\begin{aligned} \rho_0 \ddot{U}_i(\mathbf{x}, t) + \zeta \langle \rho(\mathbf{y}) H_{ikl}(\mathbf{y}) \rangle e_{xkl}(\ddot{\mathbf{U}}) + \zeta^2 \langle \rho(\mathbf{y}) P_{ijmn}(\mathbf{y}) \rangle e_{xmn}(\ddot{\mathbf{U}})_{,x_j} = \\ D_{ijmn}^0 e_{xmn}(\mathbf{U})_{,x_j} + \zeta D_{ijkmn}^1 e_{xmn}(\mathbf{U})_{,x_k x_j} + \zeta^2 D_{ijprmn}^2 e_{xmn}(\mathbf{U})_{,x_r x_p x_j}; \quad \mathbf{x} \in \Omega \end{aligned} \quad (39)$$

The terms inducing micro-inertia effects in the macroscopic equation of motion defined in Eq. 39 are scaled by orders of ζ , which leads to zero at the asymptotic limit. This appears to indicate that the contribution of the high order terms are trivial. This apparent contradiction is resolved by observing that the coefficients in these terms themselves are size dependent. It can be shown that \mathbf{D}^1 and $\langle \rho \mathbf{H} \rangle$ are proportional to \hat{l} , and \mathbf{D}^2 and $\langle \rho \mathbf{P} \rangle$ are proportional to \hat{l}^2 [9]:

$$\mathbf{D}^1 = O(\mathbf{C}\hat{l}); \quad \langle \rho \mathbf{H} \rangle = O(\rho \hat{l}) \quad (40a)$$

$$\mathbf{D}^2 = O(\mathbf{C}\hat{l}^2); \quad \langle \rho \mathbf{P} \rangle = O(\rho \hat{l}^2) \quad (40b)$$

where $\hat{l} = l/\zeta$ is the characteristic length of the microstructure in the stretched coordinate system \mathbf{y} , and l the characteristic length of microstructure in the macroscopic coordinate system \mathbf{x} . \mathbf{D}^1 , \mathbf{D}^2 , $\langle \rho \mathbf{H} \rangle$ and $\langle \rho \mathbf{P} \rangle$ are homogeneous functions of degree 1. Consequently,

$$\zeta \mathbf{D}^1 = O(\mathbf{C}l); \quad \zeta \langle \rho \mathbf{H} \rangle = O(\rho l) \quad (41a)$$

$$\zeta^2 \mathbf{D}^2 = O(\mathbf{C}l^2); \quad \zeta^2 \langle \rho \mathbf{P} \rangle = O(\rho l^2) \quad (41b)$$

In this study, $\zeta \mathbf{D}^1$, $\zeta^2 \mathbf{D}^2$, $\zeta \langle \rho \mathbf{H} \rangle$ and $\zeta^2 \langle \rho \mathbf{P} \rangle$ which are directly calculated using the physical geometric size as opposed to stretched configurations. The coefficients are therefore expressed at order $O(1)$.

4 A Simplified High Order Homogenization Model

Numerical evaluation of the equation of motion for the homogenized response as defined in Eq. 39 is complicated and non-standard. The presence of the fourth order spatial derivative of the homogeneous displacement precludes the use of the finite element method with C^0 -continuous shape functions. Alternative numerical schemes such as isogeometric analysis which possesses basis functions with higher continuity [13], finite element analysis with C^1 -continuous shape functions [26], or mixed-finite element method [6] are possible paths for directly evaluating this system.

We propose a high order homogenization model derived based on certain observations and simplifications on the material microstructures. The following conditions are assumed: (1) the homogenized material must exhibit orthotropy or higher symmetry; and (2) within a microstructural constituent domain, the elastic modulus tensor and constituent density are

assumed to be constant, but the properties are allowed to vary from constituent to constituent and generate micro-inertia under dynamic conditions. Using the first simplification, the first order stiffness tensor vanishes: $\mathbf{D}^1 = 0$ [17]. Substituting Eqs. 17, 24 and 31 into Eq. 9, taking the temporal derivative twice, premultiplying by density and averaging over the characteristic volume yields the following expression:

$$\langle \rho \ddot{u}_i \rangle = \rho_0 \ddot{U}_i(\mathbf{x}, t) + \zeta \langle \rho H_{ikl} \rangle e_{xkl}(\ddot{\mathbf{U}}) + \zeta^2 \langle \rho P_{ijkl} \rangle e_{xkl}(\ddot{\mathbf{U}})_{,x_j} + O(\zeta^3) \quad (42)$$

Comparing the differential orders in Eq. 42 to classical dispersion theories, (e.g. Mindlin's theory [25]), the second term on the right hand side is non-standard. When the assumption of piecewise constant material parameters mentioned above is considered, it has been demonstrated in [22] that the coefficient of this term is identically zero for 1-D cases. In Appendix A, it is shown that this term vanishes for high dimensional cases as well:

$$\langle \rho H_{ikl} \rangle = 0 \quad (43)$$

Next, we turn our attention to the term in Eq. 39 that involves the fourth order derivative of the homogenized displacement field. We consider the following approximation for the homogenized stiffness tensor, \mathbf{D}^2 :

$$D_{ijprmn}^2 \approx A_{ijpq} D_{qrmn}^0 \quad (44)$$

in which, \mathbf{D}^2 is taken to be proportional to \mathbf{D}^0 . Note that the approximation cannot be exactly satisfied for any \mathbf{A} . Further, since the multiplication only permutes over the fourth index, inversion of \mathbf{D}^0 for identifying \mathbf{A} is not possible. Alternatively, we employ the Moore-Penrose pseudo-inverse for identifying \mathbf{A} . Define:

$$A_{ijpq}^* = D_{ijprmn}^2 D_{qrmn}^{0 \text{ -mp}} \quad (45)$$

where '-mp' denotes the Moore-Penrose pseudo-inverse. The pseudo-inverse provides the solution, \mathbf{A}^* , that minimizes the discrepancy between \mathbf{D}^2 and its approximation, \mathbf{D}^{2*} , computed as $D_{ijprmn}^{2*} = A_{ijpq}^* D_{qrmn}^0$ with respect to the Frobenius norm. The pseudo-inverse is well defined and unique for all matrices including non-square matrices whose entries are real or complex. Additional details on the properties of Moore-Penrose pseudo-inverse are provided in Appendix B

\mathbf{A}^* possesses minor symmetry with respect to the first two indices (i.e. $A_{ijpq}^* = A_{jipq}^*$). The fourth order term in Eq. 39 is expressed as:

$$\zeta^2 D_{ijprmn}^2 e_{xmn}(\mathbf{U})_{,x_r x_p x_j} = \zeta^2 A_{ijpq}^* D_{qrmn}^0 e_{xmn}(\mathbf{U})_{,x_r x_p x_j} \quad (46)$$

Using Eq. 20 and neglecting $O(\zeta^3)$ and higher order terms:

$$\zeta^2 A_{ijpq}^* D_{qrmn}^0 (e_{xmn}(\mathbf{U}))_{,x_r x_p x_j} = \zeta^2 \rho_0 A_{ijmn}^* e_{xmn}(\ddot{\mathbf{U}})_{,x_j} \quad (47)$$

Substituting Eq. 47 to Eq. 39, the macroscale high order equation of motion becomes:

$$\rho_0 \ddot{U}_i(\mathbf{x}, t) + \zeta^2 \langle \rho P_{ijmn} \rangle (e_{xmn}(\ddot{\mathbf{U}}))_{,x_j} = D_{ijmn}^0 (e_{xmn}(\mathbf{U}))_{,x_j} + \zeta^2 \rho_0 A_{ijmn}^* e_{xmn}(\ddot{\mathbf{U}})_{,x_j} \quad (48)$$

By employing the relationship in Eq. 47, the fourth order derivative term in the equation of motion over the homogenized domain is eliminated without loss of generality. The second order influence function, \mathbf{P} , exhibits minor symmetry with respect to the first two indices only for geometrically symmetric microstructures, but is non-symmetric for arbitrary microstructures. In order to conserve angular momentum, we consider only the symmetric part of \mathbf{P} . Let:

$$J_{ijmn} = \frac{1}{2} (\langle \rho P_{ijmn} \rangle + \langle \rho P_{jimn} \rangle) \quad (49)$$

\mathbf{A}^* is decomposed into its symmetric and antisymmetric components as:

$$A_{ijkl} = \frac{1}{2} (A_{ijkl}^* + A_{ijlk}^*) \quad (50a)$$

$$B_{ijkl} = \frac{1}{2} (A_{ijkl}^* - A_{ijlk}^*) \quad (50b)$$

Using the symmetry of the strain tensor along with Eq. 50, the equation of motion for the high order homogenization model reduces to:

$$\rho_0 \ddot{U}_i = D_{ijmn}^0 (e_{xmn}(\mathbf{U}))_{,x_j} - L_{ijmn} (e_{xmn}(\ddot{\mathbf{U}}))_{,x_j}; \quad \mathbf{x} \in \Omega \quad (51)$$

where the micro-inertia induced acceleration modulus tensor, \mathbf{L} , is defined as:

$$L_{ijmn} = \zeta^2 (J_{ijmn} - \rho_0 A_{ijmn}^*) \quad (52)$$

The acceleration modulus tensor, \mathbf{L} , satisfies the minor symmetry for both the first two and the last two indices (i.e. $L_{ijmn} = L_{jimn}$; $L_{ijmn} = L_{ijnm}$). By Eqs. 49 and 50, the antisymmetric components of the micro-inertia terms in the governing equation of motion is discarded. This simplification amounts to the decomposition of the micro-inertia into transitional and rotational components, and eliminating the rotational micro-inertia effects from the formulation.

From Eq. 51, the constitutive equation for the high order model at the macroscale is defined as:

$$\Sigma_{ij}(\mathbf{x}, t) = D_{ijmn}^0 e_{xmn}(\mathbf{U}) - L_{ijmn} e_{xmn}(\ddot{\mathbf{U}}); \quad \mathbf{x} \in \Omega \quad (53)$$

where Σ is defined as the homogenized stress tensor which is related to the second order

spatial derivative of not only the homogenized displacement, \mathbf{U} , but also the acceleration, $\ddot{\mathbf{U}}$. The second term on the right hand side of Eq. 53 represents the influence of micro-inertia. The IBVP for the high order homogenization model is summarized in Box 4.

Equation 53 is obtained by substituting the fourth order spatial derivative of the displacement field with a second spatial derivative - second temporal derivative term. A one-dimensional numerical example is provided to demonstrate the impact of this substitution. The solution strategy for one-dimensional problems is provided in [22]. Consider a bi-phase one-dimensional structure with elastic moduli and density of $E^{(1)} = 2$ GPa, $\rho^{(1)} = 7900$ kg/m³ for phase 1 and $E^{(2)} = 22.4$ MPa, $\rho^{(2)} = 1070$ kg/m³ for phase 2. The volume fraction of phase 1 is 0.4. This structure consists of 20 microstructures and subjected to a step displacement load. Figure 4 illustrates the displacement histories computed using the model, which includes the fourth order spatial derivative and the model, which includes the second spatial - second temporal derivative term. The observation point is $0.1L$ distance (L is the length of the structure) from the boundary of excitation. The displacement histories indicate that the models capture the dispersion in reasonable agreement with some discrepancy in the waves following the main dispersive wave.

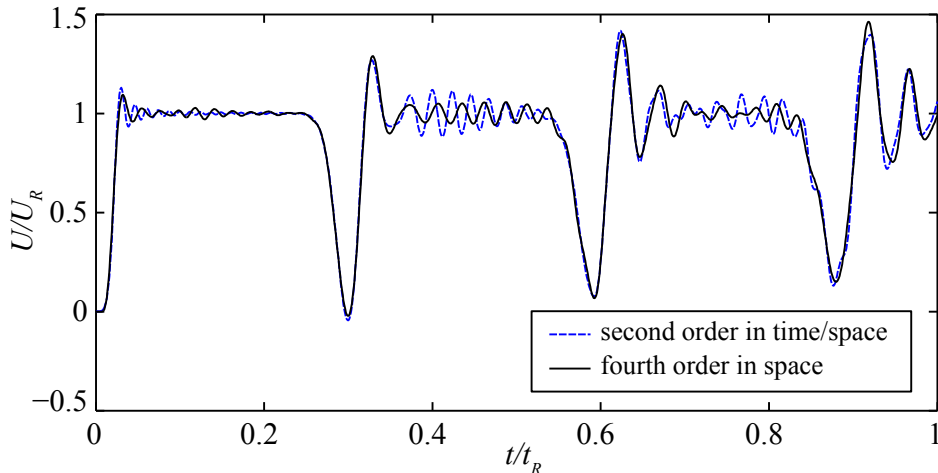


Figure 2: Displacement histories computed using a model with the fourth order spatial derivative term and a model with the second order spatial - second order temporal derivative term.

5 Finite Element Formulation

In this section, the numerical evaluations of the first and second order influence function problems defined in Boxes 1 and 3, respectively, as well as the macroscopic homogenization model defined in Box 4 are presented. The basis of the computations for all the three problems is the standard Bubnov-Galerkin finite element method with C^0 -continuous shape functions. In the evaluation of the macroscopic problem, a Hybrid Laplace Transform/Finite Element Method is proposed to solve the macroscopic IBVP.

Given: The homogenized material properties at the macroscale, \mathbf{D}^0 ; the tensor of the acceleration moduli, \mathbf{L} , initial conditions $\hat{\mathbf{u}}(\mathbf{x})$, $\hat{\mathbf{v}}(\mathbf{x})$; and the boundary conditions $\bar{\mathbf{u}}(\mathbf{x}, t)$, $\bar{\mathbf{t}}(\mathbf{x}, t)$.

Find: The macroscale deformation, $\mathbf{U}(\mathbf{x}, t) : \Omega \times [0, t_0] \rightarrow \mathbb{R}^{n_{sd}}$ such that:

- Equation of motion:

$$\rho_0 \ddot{U}_i = \Sigma_{ij,x_j}; \quad \mathbf{x} \in \Omega$$

- Constitutive relation:

$$\Sigma_{ij}(\mathbf{x}, t) = D_{ijmn}^0(e_{xmn}(\mathbf{U})) - L_{ijmn}(e_{xmn}(\ddot{\mathbf{U}})); \quad \mathbf{x} \in \Omega$$

- Boundary conditions:

$$U_i(\mathbf{x}, t) = \bar{u}_i(\mathbf{x}, t); \quad \mathbf{x} \in \Gamma^u$$

$$\Sigma_{ij}n_j = \bar{t}_i(\mathbf{x}, t); \quad \mathbf{x} \in \Gamma^t$$

- Initial conditions:

$$U_i(\mathbf{x}, 0) = \hat{u}_i(\mathbf{x}); \quad \mathbf{x} \in \Omega$$

$$\dot{U}_i(\mathbf{x}, 0) = \hat{v}_i(\mathbf{x}); \quad \mathbf{x} \in \Omega$$

Box 4: Summary of the initial boundary value problem for evaluation of the macroscale displacement, \mathbf{U} .

The computation of the first order influence function, \mathbf{H} , has been standard practice in the computational homogenization literature [21] and only a brief summary is therefore presented here for completeness. The computation of the second order influence function, \mathbf{P} , has not been a part of the traditional computational homogenization method. This section includes the detailed formulation for evaluating the second order influence function, \mathbf{P} .

5.1 First order influence function problem

Equation 18 is expressed in the weak form using the local periodicity boundary condition on $\mathbf{y} \in \Theta$ as:

$$\int_{\Theta} w_{i,y_j}(\mathbf{y}) C_{ijkl}(\mathbf{y}) h_{klmn}(\mathbf{y}) d\mathbf{y} = - \int_{\Theta} w_{i,y_j}(\mathbf{y}) C_{ijmn}(\mathbf{y}) d\mathbf{y} \quad (54)$$

where $\mathbf{w} \in \mathcal{W}_{\text{per}} \subset [H_{\text{per}}^1(\Theta)]^{n_{sd}}$; and $H_{\text{per}}^1(\Theta)$ is the subspace of functions in $H^1(\Theta)$ that are periodic along Γ_{Θ} , and $H^1(\Theta)$ is the Sobolev space of functions with square integrable derivatives. We seek the solution of the first order influence function in the finite dimensional

space, $\mathbf{H} \in \mathcal{H}_{\text{per}}(\Theta) \subset [H_{\text{per}}^1(\Theta)]^{n_{\text{sd}} \times n_{\text{sd}} \times n_{\text{sd}}}$ such that:

$$\mathcal{H}_{\text{per}}(\Theta) := \left\{ \mathbf{H}(\mathbf{y}) \mid H_{ikl}(\mathbf{y}) = \sum_{A=1}^M N^{[A]}(\mathbf{y}) H_{ikl}^{[A]}; H_{ikl}^{[A]} \text{ is } \Theta \text{-periodic; } \langle H_{ikl} \rangle = 0; H_{ikl}^{[A]} = H_{ilk}^{[A]} \right\} \quad (55)$$

with the appropriate continuity and smoothness conditions. $N^{[A]}$ denotes the shape function of node A within the discretization of the characteristic volume; M denotes the total number of nodes, and $H_{ikl}^{[A]}$ the nodal coefficients. Following the standard Bubnov-Galerkin setting, \mathcal{W}_{per} is defined similarly to Eq. 55.

Substituting the discretizations of the influence function and the weight function into the weak form and expressing the terms in matrix-vector form using the Voigt notation yields the following discrete system:

$$\mathbf{K}_H \mathbf{d}_H = \mathbf{F}_H \quad (56)$$

which is formed by assembling the element matrices:

$$\mathbf{K}_H = \mathbf{A}_e \mathbf{K}_H^e; \quad \mathbf{d}_H = \mathbf{A}_e \mathbf{d}_H^e; \quad \mathbf{F}_H = \mathbf{A}_e \mathbf{F}_H^e \quad (57)$$

\mathbf{A} denotes the assembly operation. The element matrix of unknown coefficients of an arbitrary element e is expressed as:

$$\mathbf{d}_H^e = \left[\tilde{\mathbf{H}}^{e[1]} \quad \tilde{\mathbf{H}}^{e[2]} \quad \dots \quad \tilde{\mathbf{H}}^{e[M_e]} \right]^T \quad (58)$$

in which T denotes the matrix transpose, M_e denotes the number of nodes in the element, and for 2-D elements, the matrix of unknown coefficients at node A of element e is:

$$\tilde{\mathbf{H}}^{e[A]} = \begin{bmatrix} H_{111}^{e[A]} & H_{122}^{e[A]} & H_{112}^{e[A]} \\ H_{211}^{e[A]} & H_{222}^{e[A]} & H_{212}^{e[A]} \end{bmatrix}^T \quad (59)$$

The element stiffness and force matrices are expressed as:

$$\mathbf{K}_H^e = \int_{\Theta^e} \mathbf{B}^{eT}(\mathbf{y}) \hat{\mathbf{C}} \mathbf{B}^e(\mathbf{y}) d\mathbf{y} \quad (60)$$

$$\mathbf{F}_H^e = \int_{\Theta^e} \mathbf{B}^{eT}(\mathbf{y}) \hat{\mathbf{C}} d\mathbf{y} \quad (61)$$

where Θ^e denotes the domain of element e , and

$$\mathbf{B}^e = \begin{bmatrix} \mathbf{B}^{e[1]} & \mathbf{B}^{e[2]} & \dots & \mathbf{B}^{e[M_e]} \end{bmatrix} \quad (62a)$$

$$\mathbf{B}^{e[A]} = \begin{bmatrix} N_{,y_1}^{e[A]}(\mathbf{y}) & 0 & N_{,y_2}^{e[A]}(\mathbf{y}) \\ 0 & N_{,y_2}^{e[A]}(\mathbf{y}) & N_{,y_1}^{e[A]}(\mathbf{y}) \end{bmatrix}^T \quad (62b)$$

and $\hat{\mathbf{C}}$ is the tensor of elastic moduli expressed in contracted Voigt notation.

5.2 Second order influence function problem

The weak form of Eq. 25, using the local periodicity condition, is expressed as:

$$\int_{\Theta} w_{i,y_j}(\mathbf{y}) (C_{ijkl}(p_{klpmn}(\mathbf{y}) + H_{kmn}(\mathbf{y})\delta_{lp})) d\mathbf{y} = - \int_{\Theta} w_i(\mathbf{y}) (\theta(\mathbf{y})D_{ipmn}^0 - C_{ipmn}^0(\mathbf{y})) d\mathbf{y} \quad (63)$$

for any weight function, $\mathbf{w} \in \mathcal{W}_{\text{per}}(\Theta)$. The solution approximation for the second order influence function belongs to the following finite dimensional space, $\mathbf{P} \in \mathcal{P}_{\text{per}}(\Theta) \subset [H_{\text{per}}^1(\Theta)]^{n_{\text{sd}} \times n_{\text{sd}} \times n_{\text{sd}} \times n_{\text{sd}}}$:

$$\mathcal{P}_{\text{per}}(\Theta) := \left\{ \mathbf{P}(\mathbf{y}) \mid P_{ijmn}(\mathbf{y}) = \sum_{A=1}^M N^{[A]}(\mathbf{y}) P_{ijmn}^{[A]}; P_{ijmn}^{[A]} \text{ is } \Theta \text{-periodic; } \langle P_{ijmn} \rangle = 0; P_{ijmn}^{[A]} = P_{ijnm}^{[A]} \right\} \quad (64)$$

where $P_{ijmn}^{[A]}$ denotes the nodal coefficient of \mathbf{P} at node, A . Employing the discretization of the second order influence function in Eq. 64 and the weight function, the weak form of the influence function leads to the following discrete system:

$$\mathbf{K}_P \mathbf{d}_P = \mathbf{F}_P \quad (65)$$

formed by the assembly of element matrices defined analogous to Eq. 57. \mathbf{d}_P is assembled from element matrices of unknown coefficients:

$$\mathbf{d}_P^e = \left[\tilde{\mathbf{P}}^{e[1]}, \tilde{\mathbf{P}}^{e[2]}, \dots, \tilde{\mathbf{P}}^{e[M_e]} \right]^T \quad (66)$$

For 2-D elements, the matrix of unknown coefficients at node A of element e is:

$$\tilde{\mathbf{P}}^{e[A]} = \begin{bmatrix} P_{1111}^{e[A]} & P_{1122}^{e[A]} & P_{1112}^{e[A]} & P_{1211}^{e[A]} & P_{1222}^{e[A]} & P_{1212}^{e[A]} \\ P_{2111}^{e[A]} & P_{2122}^{e[A]} & P_{2112}^{e[A]} & P_{2211}^{e[A]} & P_{2222}^{e[A]} & P_{2212}^{e[A]} \end{bmatrix}^T \quad (67)$$

The matrix of unknown nodal coefficients, \mathbf{d}_P , has 6 columns for a 2-D problem and 18 columns for a full 3-D characteristic volume. Noting that the stiffness matrix, \mathbf{K}_P , defined below does not vary as a function of the components of \mathbf{P} , the factorization of \mathbf{K}_P is conducted only once. It is also straightforward to see that the stiffness matrix for the second order influence function is identical to the stiffness matrix for the first order influence function (i.e. $\mathbf{K}_P = \mathbf{K}_H$). This further simplifies the computation of the influence functions since the factorization of only one matrix is necessary for both the first and second order influence function problems. The evaluations for the first and second order influence functions, however, are successive since the force matrix of the second order influence function depends on \mathbf{H} , (i.e. $\mathbf{F}_P = \mathbf{F}_P(\mathbf{H})$). The force matrix for element e is written as a sum of three components:

$$\mathbf{F}_P^e = \mathbf{F}_{P_1}^e + \mathbf{F}_{P_2}^e + \mathbf{F}_{P_3}^e \quad (68)$$

The first component of the force matrix is:

$$\mathbf{F}_{P_1}^e = - \int_{\Theta^e} \mathbf{B}^e(\mathbf{y})^T \hat{\mathbf{C}} \mathbf{G}(\mathbf{y}) d\mathbf{y} \quad (69)$$

where,

$$\mathbf{G} = \begin{bmatrix} H_{111}(\mathbf{y}) & H_{122}(\mathbf{y}) & H_{112}(\mathbf{y}) & 0 & 0 & 0 \\ 0 & 0 & 0 & H_{211}(\mathbf{y}) & H_{222}(\mathbf{y}) & H_{212}(\mathbf{y}) \\ H_{211}(\mathbf{y}) & H_{222}(\mathbf{y}) & H_{212}(\mathbf{y}) & H_{111}(\mathbf{y}) & H_{122}(\mathbf{y}) & H_{112}(\mathbf{y}) \end{bmatrix} \quad (70)$$

The components of \mathbf{G} is computed using the solution of the first order influence function problem within Θ^e :

$$H_{ikl}(\mathbf{y}) = \sum_{B=1}^{M_e} N^{e[B]}(\mathbf{y}) H_{ikl}^{e[B]} \quad (71)$$

The second component of the force matrix is written as:

$$\mathbf{F}_{P_2}^e = - \int_{\Theta^e} \theta \mathbf{N}^{eT}(\mathbf{y}) d\mathbf{y} \tilde{\mathbf{D}}^0 \quad (72)$$

where,

$$\tilde{\mathbf{D}}^0 = \begin{bmatrix} D_{1111}^0 & D_{1122}^0 & D_{1112}^0 & D_{1211}^0 & D_{1222}^0 & D_{1212}^0 \\ D_{1211}^0 & D_{1222}^0 & D_{1212}^0 & D_{2211}^0 & D_{2222}^0 & D_{2212}^0 \end{bmatrix} \quad (73)$$

$$\mathbf{N}^e = \begin{bmatrix} N^{e[1]} & 0 & N^{e[2]} & 0 & \dots & N^{e[M_e]} & 0 \\ 0 & N^{e[1]} & 0 & N^{e[2]} & \dots & 0 & N^{e[M_e]} \end{bmatrix} \quad (74)$$

The components of $\tilde{\mathbf{D}}^0$ then are computed after the evaluation of the first order influence function problem. Note that the matrix representation of the tensors differs from the standard

Voigt notation. The alternative notation employed here facilitates single index multiplication in the force components.

In order to evaluate the third component of the force term, we define

$$\psi_{ijkl}(\mathbf{y}) = C_{ijmn}(\mathbf{y}) \sum_{B=1}^{M_e} N_{,y_n}^{e[B]}(\mathbf{y}) H_{mkl}^{e[B]}; \quad \mathbf{y} \in \Theta^e \quad (75)$$

and denote $\hat{\boldsymbol{\psi}}$ using the Voigt representation, which is expressed as:

$$\hat{\boldsymbol{\psi}}(\mathbf{y}) = \hat{\mathbf{C}}(\mathbf{y}) \mathbf{B}^e(\mathbf{y}) \mathbf{d}_H^e \quad (76)$$

Employing the alternative notation analogous to those defined in Eqs. 73 and 74, the third component of the force term is written as:

$$\mathbf{F}_{P_3}^e = \int_{\Theta^e} \mathbf{N}^{eT}(\mathbf{y}) \left(\tilde{\boldsymbol{\psi}}(\mathbf{y}) + \tilde{\mathbf{C}}(\mathbf{y}) \right) d\mathbf{y} \quad (77)$$

in which $\tilde{\boldsymbol{\psi}}$ and $\tilde{\mathbf{C}}$ are the alternative matrix representation of $\boldsymbol{\psi}$ and \mathbf{C} , respectively:

$$\tilde{\boldsymbol{\psi}} = \begin{bmatrix} \psi_{1111} & \psi_{1122} & \psi_{1112} & \psi_{1211} & \psi_{1222} & \psi_{1212} \\ \psi_{1211} & \psi_{1222} & \psi_{1212} & \psi_{2211} & \psi_{2222} & \psi_{2212} \end{bmatrix} \quad (78)$$

$$\tilde{\mathbf{C}} = \begin{bmatrix} C_{1111} & C_{1122} & C_{1112} & C_{1211} & C_{1222} & C_{1212} \\ C_{1211} & C_{1222} & C_{1212} & C_{2211} & C_{2222} & C_{2212} \end{bmatrix} \quad (79)$$

5.3 Macroscopic problem

The weak form of Eq. 51 is:

$$\int_{\Omega} \rho_0 w_i \ddot{U}_i d\mathbf{x} - \int_{\Omega} w_{i,x_j} L_{ijmn} e_{xmn}(\ddot{\mathbf{U}}) d\mathbf{x} + \int_{\Omega} w_{i,x_j} D_{ijmn}^0 e_{xmn}(\mathbf{U}) d\mathbf{x} = \int_{\Gamma^t} w_i \Sigma_{ij} n_j d\mathbf{x} \quad (80)$$

for any weight function \mathbf{w} . The solution approximation for the homogenized displacement field belongs to the following finite dimensional space: $\mathbf{U} \in \mathcal{U}(\Omega)$

$$\mathcal{U}(\Omega) := \left\{ \mathbf{U}(\mathbf{x}, t) \mid U_i(\mathbf{x}, t) = \sum_{[C]=1}^K N^{[C]}(\mathbf{x}) U_i^{[C]}(t); U_i^{[C]}(t) = \bar{u}_i^{[C]}(t) \text{ when } \mathbf{x} \in \Gamma^u \right\} \quad (81)$$

where $N^{[C]}$ denotes the shape function of node C within the discretization of Ω ; $U_i^{[C]}$ the nodal displacement and K the total number of nodes. Employing the discretization of the displacement field in Eq. 81 and the weight function, the weak form of the displacement leads to the following discrete system:

$$(\mathbf{M} + \mathbf{K}_L) \ddot{\mathbf{d}}_U(t) + \mathbf{K} \mathbf{d}_U(t) = \mathbf{F}(t) \quad (82)$$

which is formed by the assembly of pertinent element matrices:

$$\mathbf{M} = \mathbf{A}_e \mathbf{M}^e; \quad \mathbf{K}_L = \mathbf{A}_e \mathbf{K}_L^e; \quad \mathbf{K} = \mathbf{A}_e \mathbf{K}^e; \quad \mathbf{F}(t) = \mathbf{A}_e \mathbf{F}^e(t) \quad (83)$$

$\mathbf{d}_U(t)$ is assembled from the element matrix of unknown coefficients:

$$\mathbf{d}_U^e = \left[\tilde{\mathbf{U}}^{e[1]}(t) \quad \tilde{\mathbf{U}}^{e[2]}(t) \quad \dots \quad \tilde{\mathbf{U}}^{e[K_e]}(t) \right]^T \quad (84)$$

where K_e denotes the number of the element nodes. For 2-D elements:

$$\tilde{\mathbf{U}}^{e[C]} = \left[U_1^{e[C]}(t) \quad U_2^{e[C]}(t) \right] \quad (85)$$

at node C in Ω^e . The element mass, acceleration, stiffness and force matrices are expressed respectively as:

$$\mathbf{M}^e = \int_{\Omega^e} \rho_0 \mathbf{N}^{eT}(\mathbf{x}) \mathbf{N}^e(\mathbf{x}) d\mathbf{x} \quad (86a)$$

$$\mathbf{K}_L^e = - \int_{\Omega^e} \mathbf{B}^{eT}(\mathbf{x}) \hat{\mathbf{L}} \mathbf{B}^e(\mathbf{x}) d\mathbf{x} \quad (86b)$$

$$\mathbf{K}^e = \int_{\Omega^e} \mathbf{B}^{eT}(\mathbf{x}) \hat{\mathbf{D}}^0 \mathbf{B}^e(\mathbf{x}) d\mathbf{x} \quad (86c)$$

$$\mathbf{F}^e = \int_{\Gamma^{et}} \mathbf{N}^{eT}(\mathbf{x}) \bar{\mathbf{t}}^e(\mathbf{x}, t) d\mathbf{x} \quad (86d)$$

where $\hat{\mathbf{D}}^0$ and $\hat{\mathbf{L}}$ are the tensors of the zeroth homogenized elastic moduli and acceleration moduli in contracted Voigt notation respectively.

Time domain integration of Eq. 82 is not straightforward. This is because the mass matrix ($= \mathbf{M} + \mathbf{K}_L$) includes the constitutive response, and mass lumping for explicit time integration would alter the constitutive response. Application of traction boundary condition is also difficult since the stress is a function of the acceleration gradient, in addition to the strain. In this manuscript, the homogenized balance equations are evaluated in the Laplace domain to alleviate the problems in the time integration and the application of traction boundary conditions. The Hybrid Laplace Transform/Finite Element Method [10, 28] is used to solve the macroscopic IBVP. The governing equations are converted from the time domain to the complex form in the Laplace domain.

The Laplace transform of an arbitrary, real valued, time varying function, $f \in \mathbb{R}$, is defined as:

$$\mathcal{F}(s) \equiv \mathcal{L}(f(t)) = \int_0^\infty e^{-st} f(t) dt \quad (87)$$

where, the Laplace argument, s and the Laplace transform, \mathcal{F} , are complex valued (i.e., $s \in \mathbb{C}$ and $\mathcal{F} := \mathbb{C} \rightarrow \mathbb{C}$). The representation of a field in the Laplace domain is referred to as the

associated field. The derivative rule for the Laplace transform is given as:

$$\mathcal{L}(\underbrace{f, tt \dots t}_{n \text{ times}}(t)) = s^n \mathcal{F}(s) - s^{n-1} f(0) - \dots - \underbrace{f, tt \dots t}_{n-1 \text{ times}}(0) \quad (88)$$

Considering statically undeformed initial conditions (i.e., $\hat{u}_i(\mathbf{x}) = \hat{v}_i(\mathbf{x}) = 0$), Eq. 82 is transformed to the complex form in the Laplace domain as:

$$(\mathbf{M}s^2 + \mathbf{K}_L s^2 + \mathbf{K}) \mathbf{d}_U^{\mathcal{L}}(s) = \mathbf{F}^{\mathcal{L}}(s) \quad (89)$$

where $\mathbf{F}^{\mathcal{L}}$ is the force vector in the Laplace domain, assembled from the element force vectors:

$$\mathbf{F}^{e\mathcal{L}} = \int_{\Gamma^{et}} \mathbf{N}^{eT} \bar{\mathbf{t}}^{e\mathcal{L}}(\mathbf{x}, s) d\mathbf{x} \quad (90)$$

Eq. 89 can be evaluated by the standard solution of linear complex equations. The constitutive relation in the Laplace domain is obtained by applying the Laplace transform to Eq. 53:

$$\Sigma_{ij}^{\mathcal{L}}(\mathbf{x}, s) = (D_{ijmn}^0 - L_{ijmn} s^2) e_{xmn}(\mathbf{U}^{\mathcal{L}}); \quad \mathbf{x} \in \Omega \quad (91)$$

in which, $\Sigma^{\mathcal{L}}$ is the associated homogenized stress. The complex fields are converted to the time domain using the numerical inverse Laplace transform (NILT) method. The NILT method employed in this work is based on Fast Fourier Transform and the ϵ -error algorithm to transform the associate fields from the complex functions to the real valued functions. Details on the numerical inverse Laplace transform method are discussed in [22].

6 Numerical Verification

A series of simulations were conducted to assess the validity of the proposed high order model and investigate the wave dispersion phenomena induced by micro-heterogeneities. The capability of the high order model is verified against the direct finite element analysis (direct FEA) solution, in which all heterogeneities are fully resolved throughout the macro-domain. The direct FEA simulations use the explicit time integration with time step sizes significantly smaller than the stability limit to ensure high accuracy. The high order method is also compared to the standard 'local' homogenization solution to determine the effects of micro-inertia on the overall responses. The local homogenization includes a two-term asymptotic expansion of the response fields resulting in the IBVP defined in Box 2. The local homogenization solution requires the computation of only the first order influence function, \mathbf{H} , which is used to compute the homogenized moduli tensor, \mathbf{D}^0 .

The examples described below focus on the investigation of microstructural wave dispersions induced only by the contrast of constituent densities since one of the unique contributions of the proposed high order homogenization model is capturing this effect. Using this model,

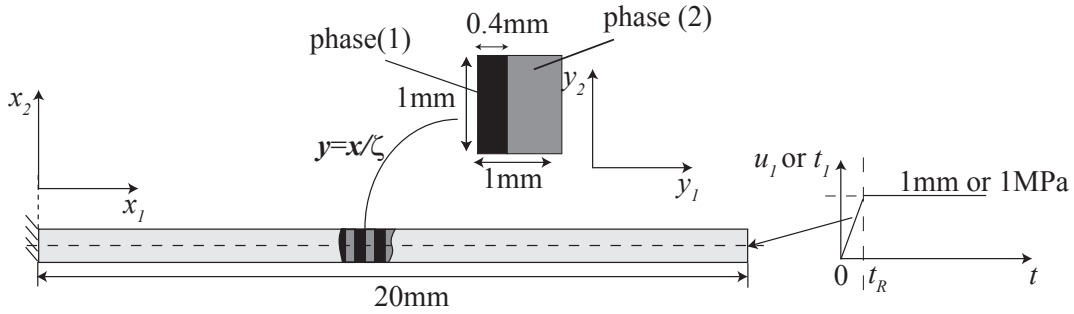


Figure 3: Configuration of the bimaterial bar under ramped step loading.

it is also possible to capture wave dispersion phenomena induced by stiffness contrast, or, in more general terms, micro-constituent impedances.

6.1 Wave propagation along a slender bar

We consider a 2-D bi-material bar subjected to a clamped constraint at its left end and loading at its right end as shown in Fig. 3. The applied loading (displacement or traction) is tensile and along the direction of the bar. The properties of the two constituent phases are chosen as $E^{(1)} = 2\text{GPa}$, $\rho^{(1)} = 7090\text{kg/m}^3$, $\nu = 0.3$ and $E^{(2)} = 2\text{GPa}$, $\rho^{(2)} = 1070\text{kg/m}^3$, respectively. The Poisson's ratio of both constituents are set to $\nu = 0.3$.

In the first set of simulations, a displacement controlled ramp loading with the maximum amplitude of 1mm is applied. The time to the maximum displacement is $t_R = 10^{-6}\text{s}$. Figure 4 shows the lateral displacement (U_1) versus time from four locations along the center line of the bar at the distance of 2, 5, 10, and 15 mm measured from the fixed end of the bar. The displacement histories for these four points computed using the direct FEA solution and the proposed high order homogenization model are compared. Since the direct FEA solution resolves the microstructure throughout the length of the bar, the reported displacement is the average displacement computed over the microstructure within which the point is located. The large peaks correspond to the traveling macroscopic wave, whereas the oscillations are due to dispersion. The dispersion in the current example (and in many other multidimensional problems with a finite domain) is not only due to the microstructural boundaries, but also due to the exterior boundaries. Simulations in the next section attempts to reduce the free boundary effects to isolate the dispersion induced only by density contrast. The displacement recorded closer to the fixed end (e.g. Fig. 4a) remains around the peak applied displacement (i.e. 0.01mm) for a shorter duration than those recorded closer to the free end. This is because the duration for the wave front to travel forth and back (reversing the sign at the fixed end) is shorter when the observation point is closer to the fixed end. All four plots in Fig. 4 demonstrate that the proposed high order homogenization model is in very reasonable agreement with the direct FEA solution in capturing the wave dispersions. While the amplitudes of the

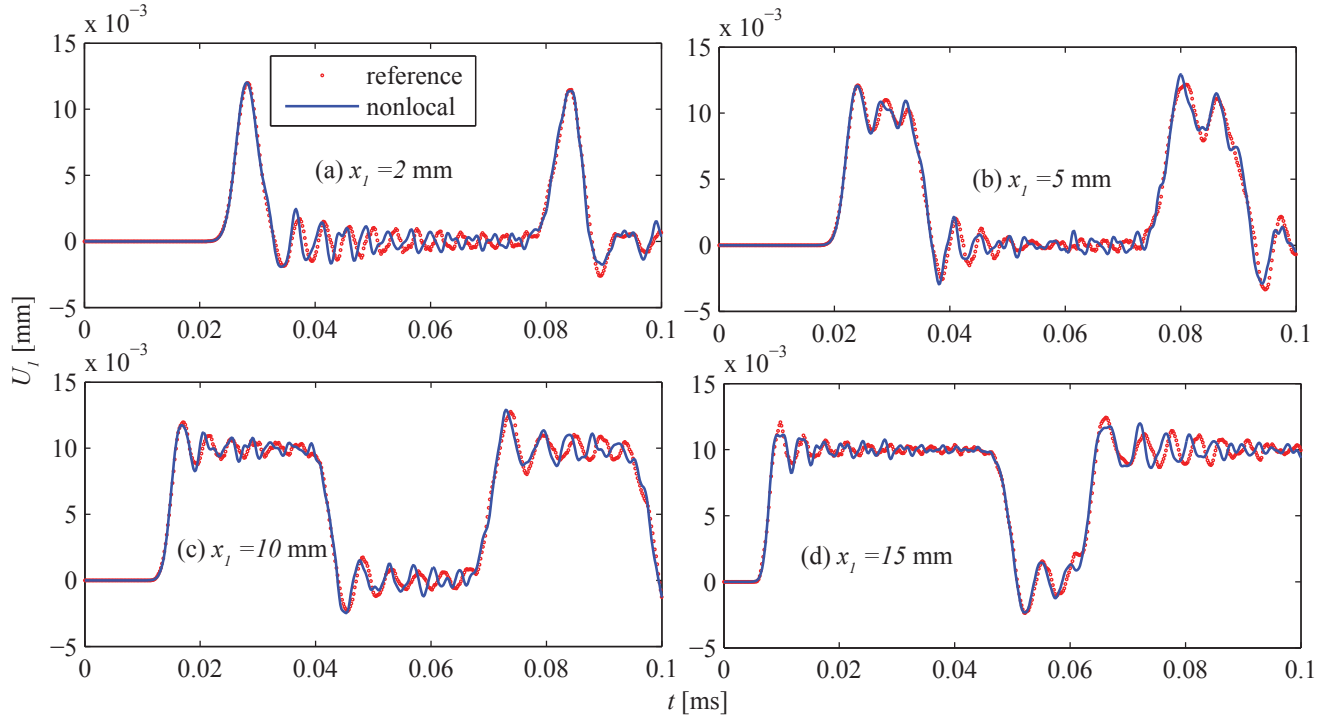


Figure 4: Displacement histories at different positions of the beam.

dispersive waves match very well, a small phase shift is observed particularly in Figs. 4a and 4b. This shift is attributed to a slight error in the propagation velocity change induced by dispersion. Figure 5 illustrates the structural view of the wave propagation through snapshots of the deformed bar at the four different time steps. The propagating wave front indicated by the sharp change in color, the wave dispersion is clearly observed by the changes in an alternating bright and loom pattern immediately following the wavefront.

In the second set of simulations, a traction controlled ramp loading with the maximum amplitude of 1MPa is applied. The time to the maximum amplitude loading is $t_R = 10^{-6}$ s. The four observation points are the same as the previous set of simulations. Figure 6 shows the lateral displacement (U_1) versus time from the four locations computed by the high order homogenization model and the direct FEA solution. The predictions given by the high order model are very similar to the direct FEA solution, demonstrating that the high order homogenization works well with the traction boundary condition as well.

6.2 Wave propagation in a square composite medium

The second example considers the dynamic response of a two-dimensional square heterogeneous medium with a layered configuration. In this example, the effect of loading frequency on the wave propagation characteristics is investigated. Two cases of wave propagation are considered as illustrated in Fig. 7. In the first set of simulations, the domain is clamped at the left edge and subjected to the displacement controlled sinusoidal stimulation at the middle of the right edge.

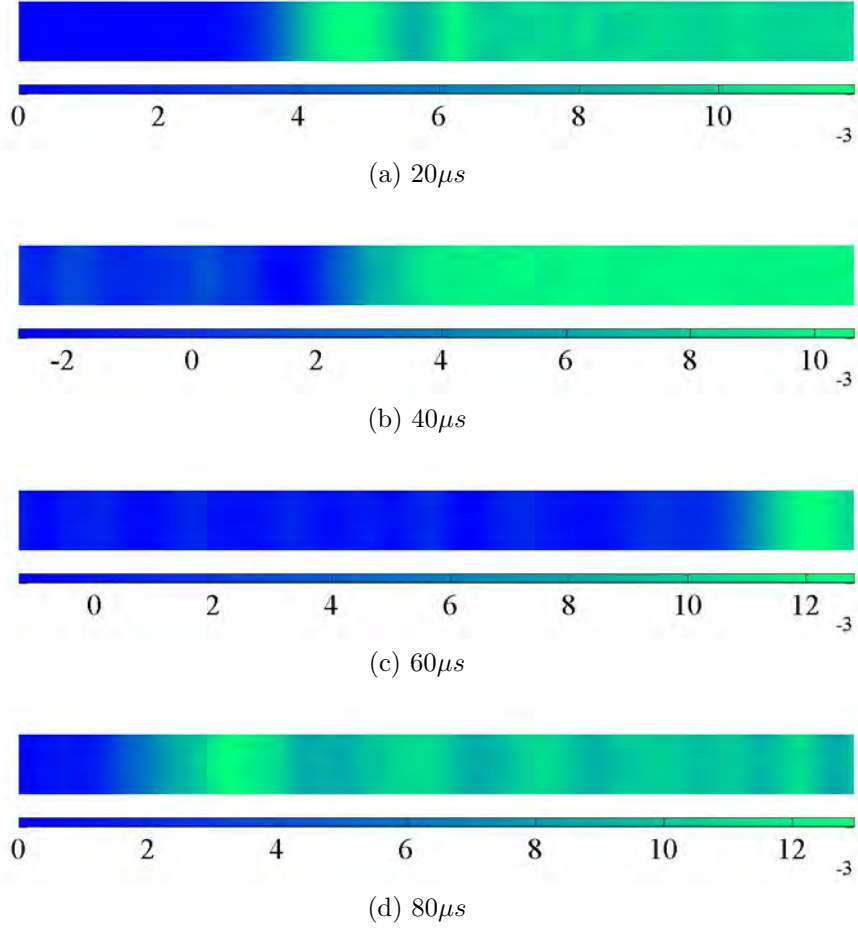


Figure 5: Structural view of U_1 [mm].

The maximum amplitude of the loading is $u_R = 0.01\text{mm}$. The shape of the domain is chosen so that the effect of boundary dispersion is relatively small compared to the dispersion induced by the microstructure. The material properties of the layers are identical to those presented in Section 6.1. The time duration of the simulations is $t_0 = 500 \mu s$. The total number of load cycles within the duration of the simulation is denoted as $N (= t_0/t_R)$. For comparison purposes, the wavelength is approximated using the p-wave speed ($= \sqrt{(\lambda_0 + 2\mu_0)/\rho_0}$, where λ_0 and μ_0 are the homogenized Lamé constants respectively and ρ_0 the homogenized density of the microstructure). The approximate wavelengths for $N=2, 12$, and 38 are $12, 3.5$ and 1.1 times the microstructural size ($=10 \text{ mm}$) respectively.

The high order homogenization, direct FEA, and the local homogenization solutions are compared in Fig. 8 for $N = 2$. The displacement contours within the problem domain are plotted at four time instances (i.e., $t = 100, 200, 300$ and $400 \mu s$). The high order homogenization, local homogenization and the direct FEA solutions provide near identical displacement profiles throughout the loading history. The similarity between the high order and local homogenization results indicates that the microstructural inhomogeneities have little influence

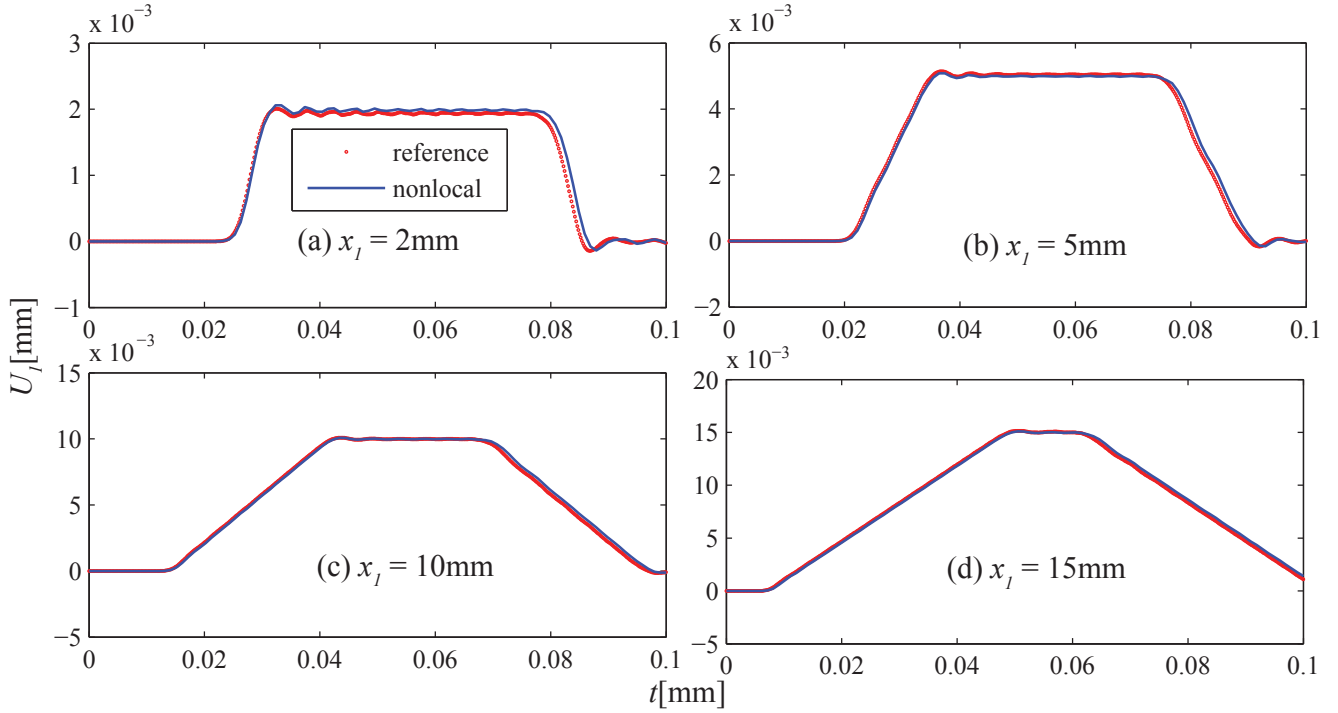


Figure 6: Displacement histories at different positions of the beam.

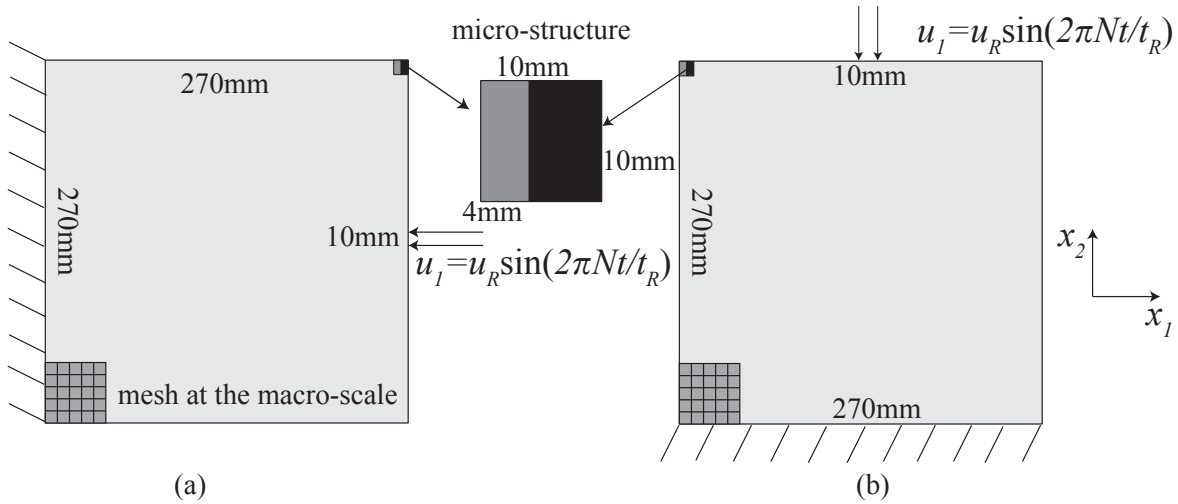


Figure 7: Configuration of the composite square under sinusoidal loading conditions: (a) wave imparted along the direction perpendicular to the layers; (b) wave imparted along the direction parallel to the layers.

on the structural response. When $N = 2$, the length of the propagating wave is large enough that the dispersion due to micro-heterogeneities (i.e. the density contrast) is negligible.

Figure 9 shows the comparison of the solutions computed by the proposed high order homogenization approach, the local homogenization and the direct FEA when $N = 12$. In these simulations, the wavelength is approximately 3.5 times the size of the microstructure. The

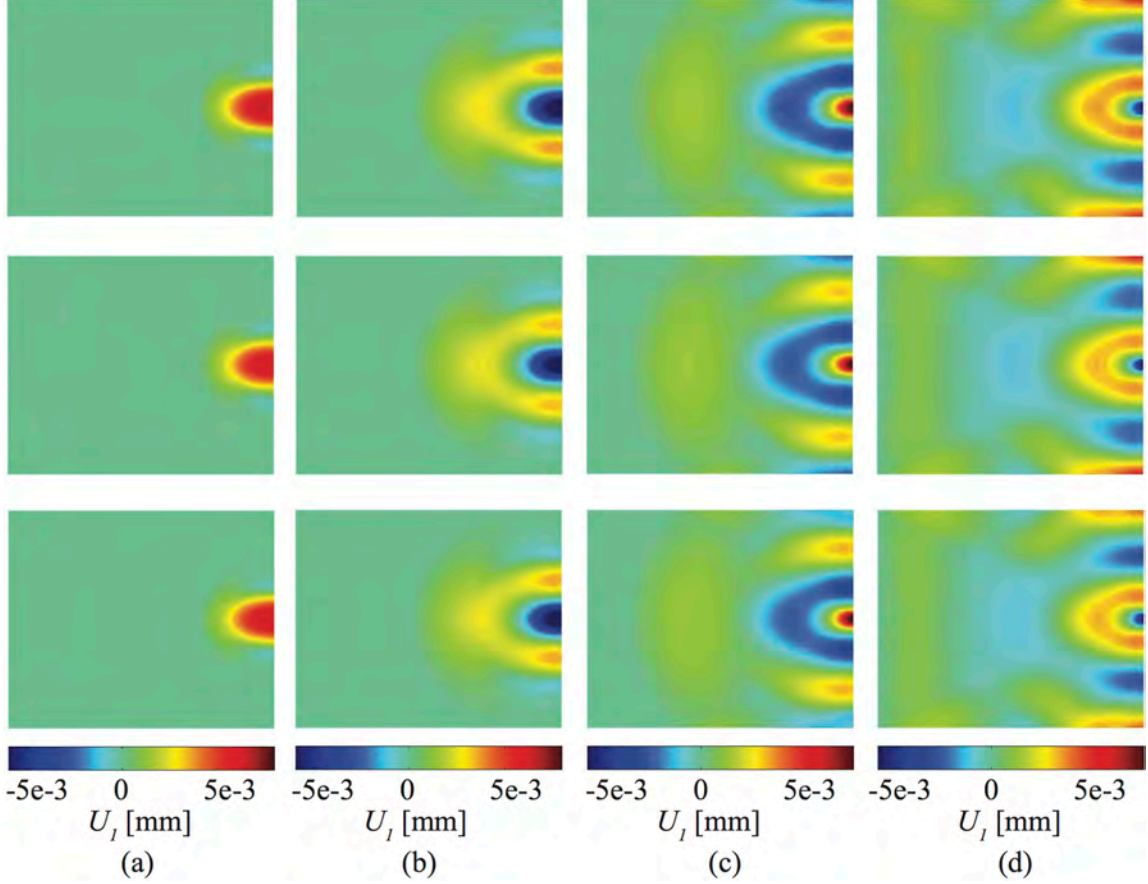


Figure 8: High order homogenization (top row), direct FEA (middle row) and the local homogenization (bottom row) solutions when $N = 2$: (a) $t = 100\mu s$; (b) $t = 200\mu s$; (c) $t = 300\mu s$; and (d) $t = 400\mu s$.

displacement profiles of the high order and local homogenization models start to deviate from each other, pointing to the presence of dispersive waves. The displacement profiles computed using the direct FEA show some deviation from the results of the high order homogenization model. While the high order homogenization model point to the localization of the wave propagation towards the center line, the direct FEA model predicts localization of the wave along two angled paths, in addition to the center line. We speculate that the angled paths are due to the interaction effects between the external boundary and the layered microstructure. The discrepancy between the displacement profiles are therefore attributed to difficulty in capturing this interaction effect using the homogenization models.

The high order homogenization, the local homogenization and the direct FEA solutions for $N = 38$ are summarized in Fig. 10. In this case, the wavelength is 1.1 times the microstructure size. The high order homogenization model shows that the wave quickly attenuates, suggesting phononic stop band behavior. In contrast, the direct FEA and the local homogenization solutions display wave propagation in the media. When the wave frequency is within the stop band, the wave vectors become complex valued [1, 33]. The direct FEA, which takes into

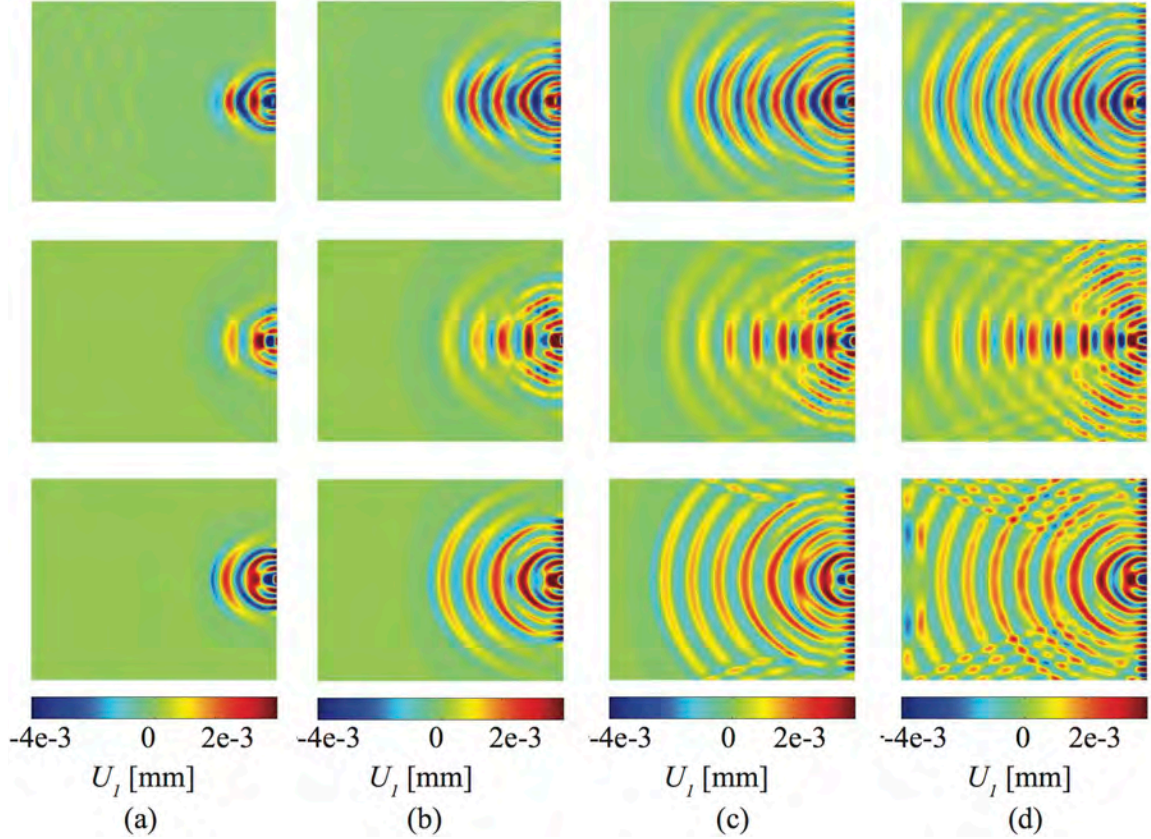


Figure 9: High order homogenization (top row), direct FEA (middle row) and the local homogenization (bottom row) solutions when $N = 12$: (a) $t = 100\mu s$; (b) $t = 200\mu s$; (c) $t = 300\mu s$; and (d) $t = 400\mu s$.

account only the real component of the wave vector, cannot adequately capture the deformation behavior accurately. Outside the stop band, the wave vectors are real valued, and therefore FEA can capture the wave propagation response provided that the domain is discretized with fine enough resolution. Fig. 11 shows U_1 along the horizontal center line of the model at frequencies $N = 2, 12$ and 38 at $t = 400\mu s$ computed using the direct FEA. Despite significant suppression of the wave amplitude, a spurious positive deformation is produced in the FEA solution. The hybrid Laplace Transform/Finite Element method employed in the evaluation of the high order homogenization model retains the imaginary component of the response, and able to simulate the stop band behavior. The wave attenuation due to the complex wave properties is included in the solution in the Laplace domain. The theoretical model proposed by Andrianov et al. [1] was used to estimate the onset of the stop band, computed as the wave frequency that leads to zero group velocity. The theoretical estimate of $N = 38$ verifies that the proposed model is reasonably accurate in predicting the onset of the stop band behavior.

In the second set of simulations, the domain is clamped at the bottom edge and subjected to the displacement controlled sinusoidal stimulation at the middle of the top edge as illustrated in Fig. 7b. The maximum amplitude of the loading is $u_R = 0.01\text{mm}$. In this example, the wave

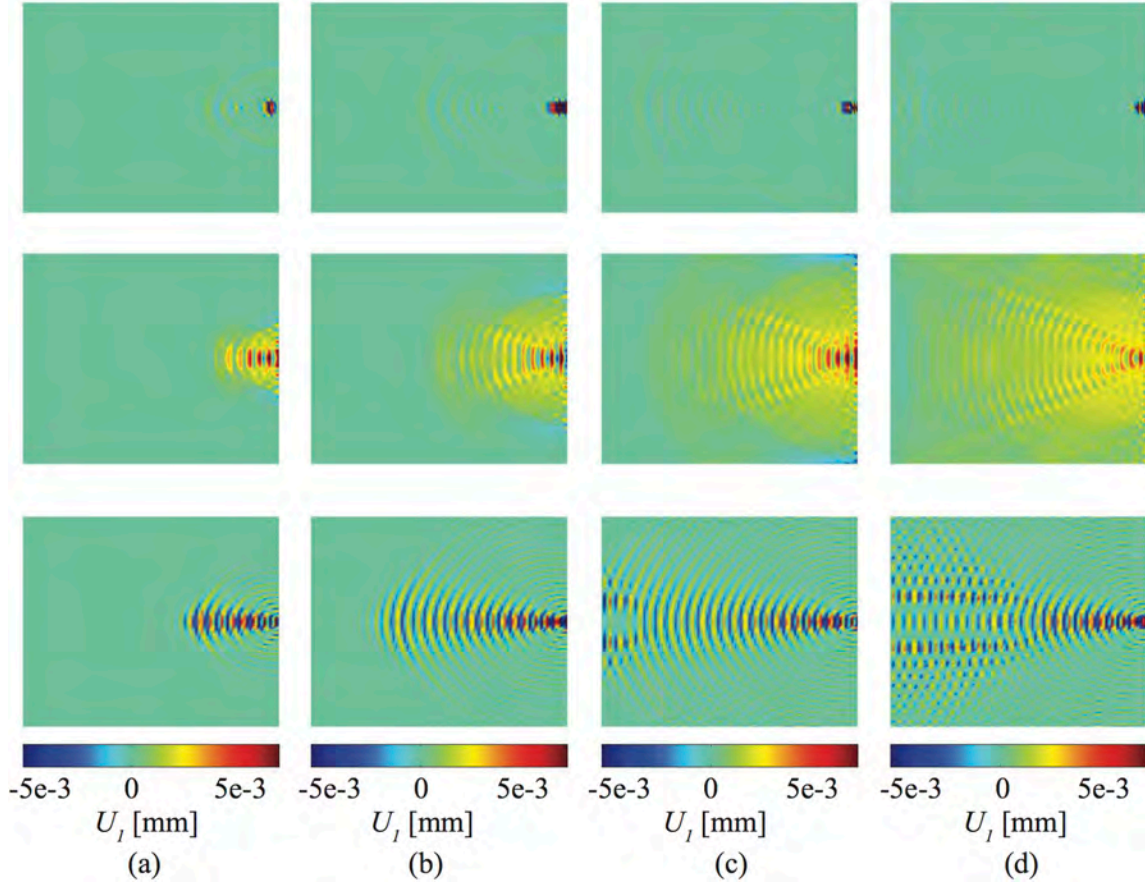


Figure 10: High order homogenization (top row), direct FEA (middle row) and the local homogenization (bottom row) solutions when $N = 38$: (a) $t = 100\mu\text{s}$; (b) $t = 200\mu\text{s}$; (c) $t = 300\mu\text{s}$; and (d) $t = 400\mu\text{s}$.

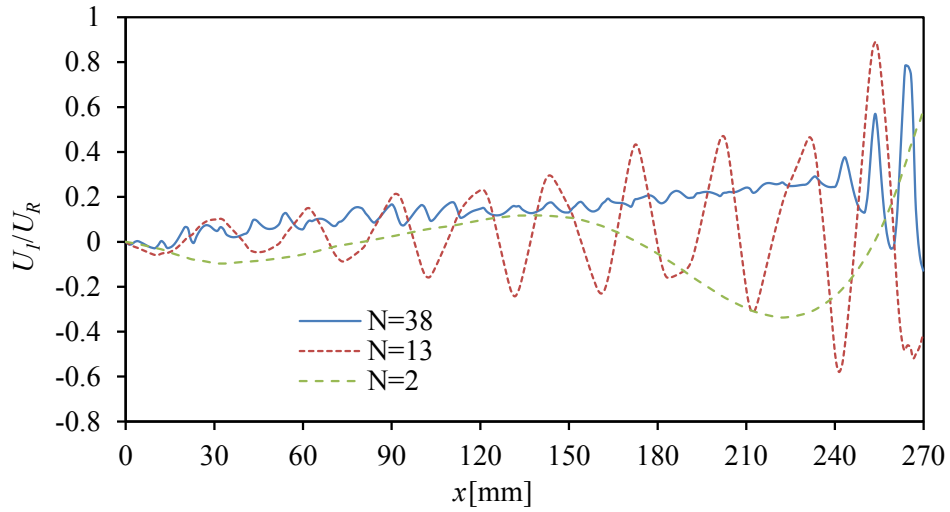


Figure 11: Direct FEA solutions of U_1 along the horizontal center lines at $t = 400\text{ms}$.

is imparted along the vertical direction, whereas the microstructure-induced dispersion impart waves along the horizontal direction. The time duration of the simulations is $t_0 = 500\mu s$. For comparison purposes, the wavelength is approximated using the shear wave speed ($= \sqrt{\mu_0/\rho_0}$). The calculated wavelengths are 10, 1.4 and 0.8 times the microstructure size for $N = 2, 15,$ and 25 cases, respectively.

Figure 12 compares the displacement contours computed by the high order, direct FEA and the local homogenization models for $N = 2$. Similar to the previous set of simulations (i.e., Fig. 8), the high order homogenization, local homogenization and the direct FEA solutions provide near identical displacement profiles throughout the loading history for long wavelengths.

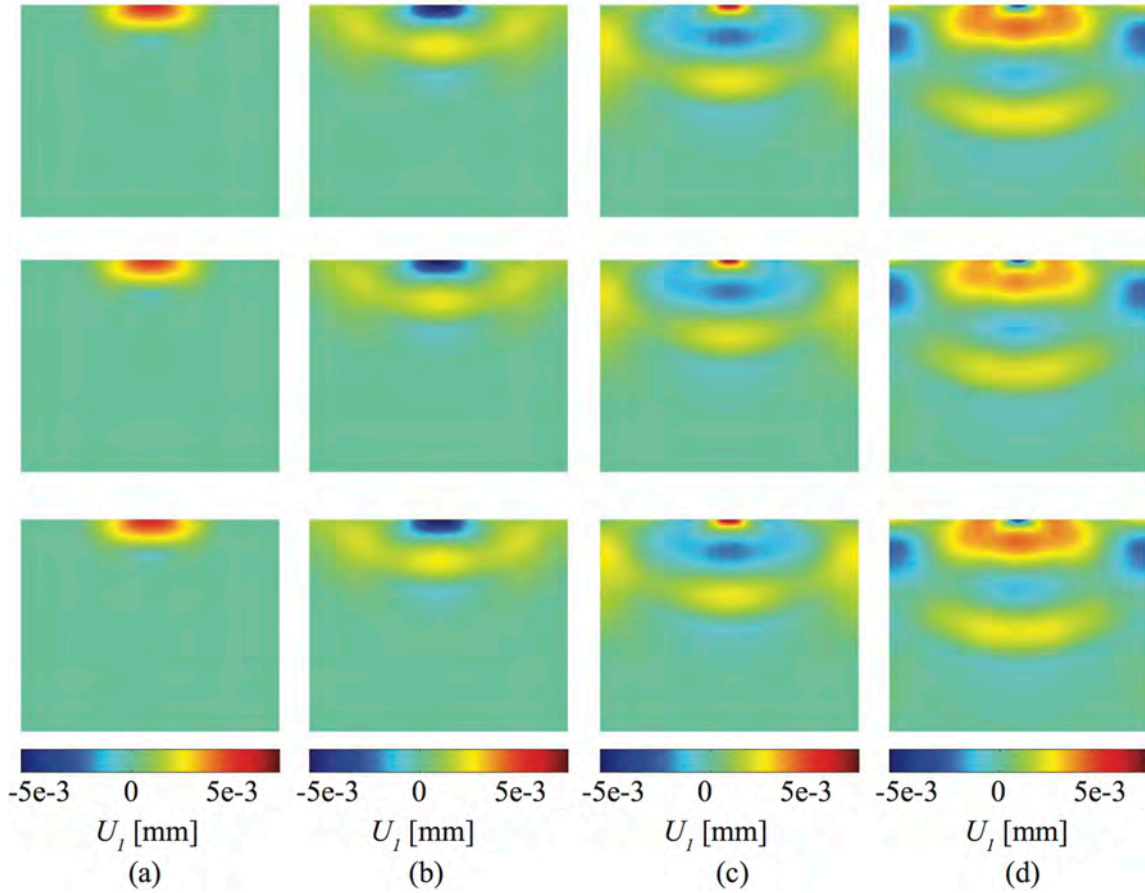


Figure 12: High order homogenization (top row), direct FEA (middle row) and the local homogenization (bottom row) solutions when $N = 2$: (a) $t = 100\mu s$; (b) $t = 200\mu s$; (c) $t = 300\mu s$; and (d) $t = 400\mu s$.

Figure 13 shows the comparison of the solutions computed by the proposed approach, the direct FEA and the local homogenization method when $N = 15$. The displacement profiles suggest that the group velocity computed by the high order homogenization and the direct FEA models is markedly lower than the local homogenization solution, indicating the effect of dispersion induced by micro-inertia. The amount of slowdown computed by the high order

homogenization and the direct FEA models are similar notwithstanding some dissimilarities between the wave patterns. The deviation from symmetry in the direct FEA results is due to the fact that the load is applied in a slightly asymmetric fashion. The vertical load is imparted on the specimen at the top of the central unit cell. The layers immediately to the right and left of the loading are therefore different (i.e., a hard and a soft layer, respectively), leading to the asymmetry observed in the direct FEA results.

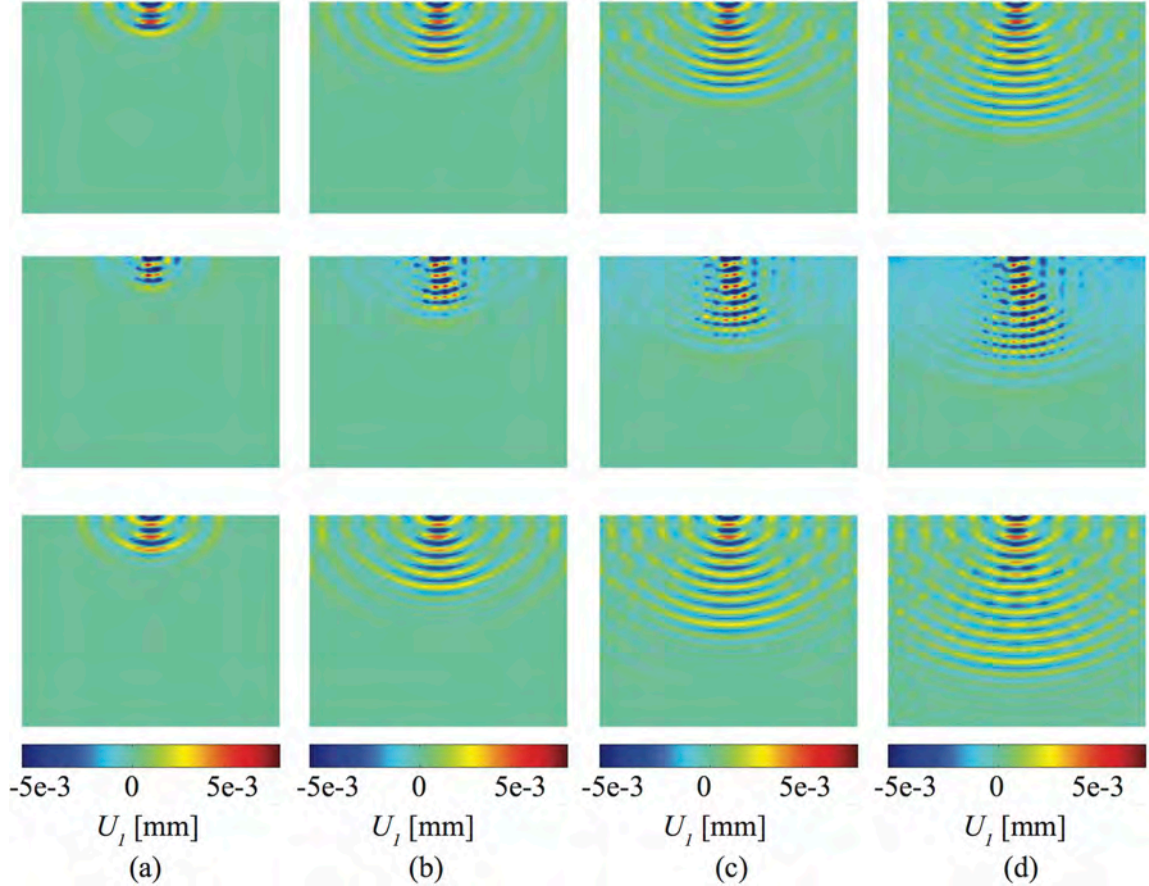


Figure 13: High order homogenization (top row), direct FEA (middle row) and the local homogenization (bottom row) solutions when $N = 15$: (a) $t = 100\mu s$; (b) $t = 200\mu s$; (c) $t = 300\mu s$; and (d) $t = 400\mu s$.

When the applied displacement frequency is further increased ($N = 25$), the high order homogenization model predicts the onset of the phononic stop band and the wave ceases to propagate significantly along the lateral direction (i.e., along the x_1 -direction). The comparison of the displacement profiles computed by the three models is shown in Fig. 14. The local homogenization model displays no effect of dispersion in this case and the wave propagation characteristics are similar to the $N = 15$ case. The FEA simulation displays a spurious residual displacement field along the lateral direction, similar to Fig. 11 described in the first set of simulations (in this case, negative displacement). The direct FEA and the high order homogenization models predict that the displacement wave continues to propagate along

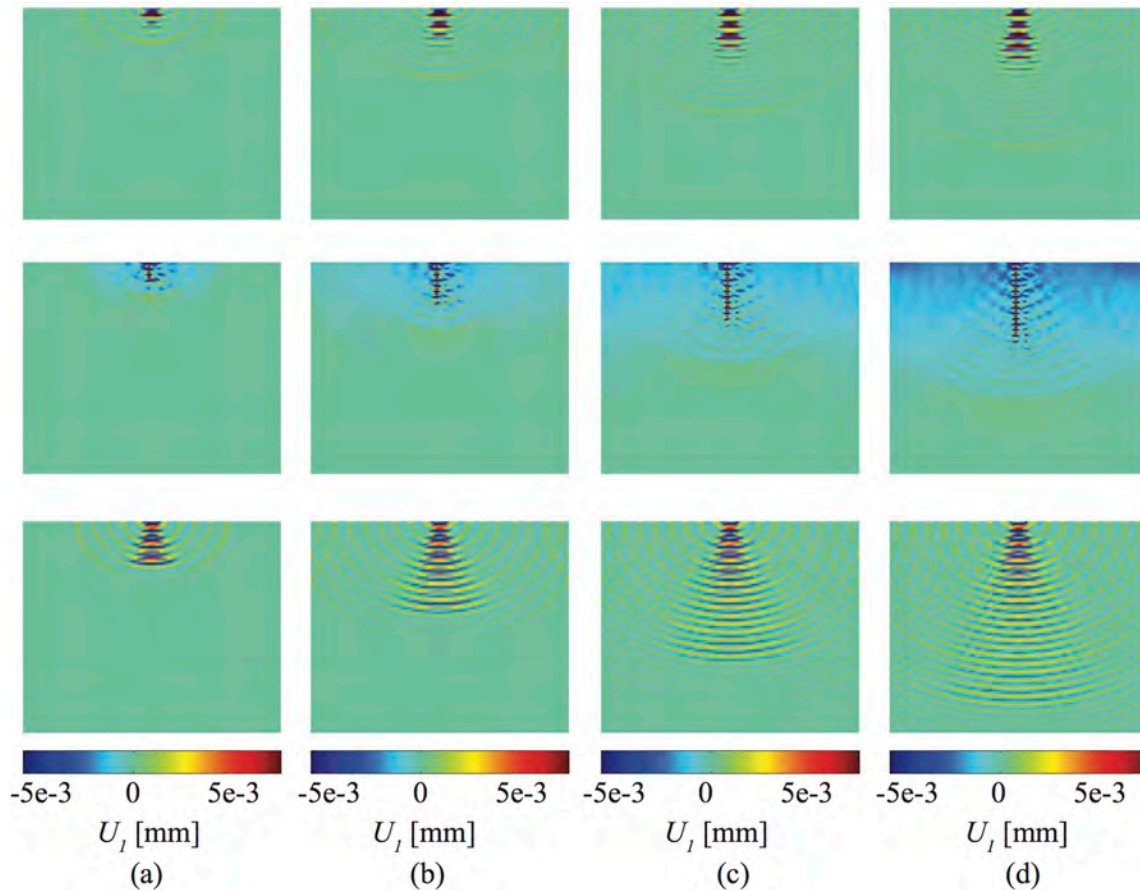


Figure 14: High order homogenization (top row), direct FEA (middle row) and the local homogenization (bottom row) solutions when $N = 25$: (a) $t = 100\mu s$; (b) $t = 200\mu s$; (c) $t = 300\mu s$; and (d) $t = 400\mu s$.

the vertical direction immediately under the prescribed boundary. This is because the wave propagation in the vertical direction occurs within the narrow band of uniform material without interference, even when the wave frequency falls into the stop band.

6.3 Computational efficiency

The computational efficiency is significantly improved using the high order homogenization model compared to the direct finite element simulation. The homogenization contributes to the computational performance. In the second numerical example, 2916 elements are used in the discretization of the macroscopic problem by the high order homogenization model, while 18225 elements are used to discretize the domain using the direct finite element simulation. The direct simulation needs many more elements to mesh the composite microstructures particularly when there is a large discrepancy between the sizes of micro- and macrostructure. Meshing the macroscopic model using the high order homogenization homogenization is independent of microstructures since the macrostructure is solved using a homogenization model. The

computation of the microstructural properties is required but only for once and off-line, so that it doesn't contribute to the computational complexity of the structural analysis.

In addition, solving the problem in the Laplace domain took 500 steps of computation by the high order homogenization model while at least 10000 time steps are required to guarantee the computational precision by the direct FEA solution. The Laplace transform converts the problem from the time domain to a complex frequency domain where as long as sufficient frequencies are captured, the solution is solved accurately. The direct FEA solution which uses the finite difference method has to make each time step small enough to remain stable and retain high accuracy. In many problems, the number of frequencies required is much smaller than the number of time steps required for stable computations.

7 Conclusions

This manuscript presented a high order homogenization computational homogenization model for simulating the dynamic response of elastic composite materials. The proposed model is derived based on the mathematical homogenization with multiple spatial scales. Higher order asymptotics have been introduced to capture the micro-inertia effects caused by the impedance contrast between the microstructural constituents. The finite element formulation for the evaluation of the microscale influence functions and the homogenized model are provided. The proposed high order homogenization model is validated by comparing against the direct finite element solutions and the local homogenization model.

From the modeling perspective, the high order homogenization model has a number of distinctions compared to the previous homogenization models (e.g. Fish et al. [17]). First, the high order homogenization model proposed in the current manuscript is able to capture the dispersion induced by the density contrast at the microscale. In all of the simulations provided in this manuscript, dispersion is induced by the density contrast (the elastic properties are taken to be the same in all constituents). Second, the proposed model is able to capture the wave propagation behavior within the phononic stop band. The appearance of stop bands in the high frequency range is due to the complex components of the wave which leads to an exponential attenuation. In the proposed model, the ability to model wave propagation within the stop band stems from the complex treatment of the response fields. The macroscale problem is evaluated in the Laplace domain where all the response fields are complex and the solution is based on the corresponding complex frequencies.

From the computational perspective, several challenges remain that will be addressed in the near future. First, the current formulation is limited to the elastic composite constituents. The formulation will be extended to include viscoelastic composites. This extension will broaden the range of applicability of the proposed model to polymeric materials, many of which exhibits significant dissipation during dynamic loading. The viscoelasticity of the constituents leads to wave attenuation by means of dispersion, which provides an additional mechanism of vibration

control and impact/blast load survivability in heterogeneous materials. The second, and bigger, challenge is the extension of the proposed model to account for failure processes. This is a significant computational undertaking, since the microstructure problems that are used to evaluate the influence function are nonlinear and need to be recomputed repeatedly throughout a macrostructure simulation. In the presence of history-dependent, nonlinear failure processes, Laplace transformations cannot be employed in a straightforward fashion.

References

- [1] I. V. Andrianov, V. I. Bolshakov, V. V. Danishevs'kyi, and D. Weichert. Higher order asymptotic homogenization and wave propagation in periodic composite materials. *Proc. R. Soc. Lond. A*, 464:1181–1201, 2008.
- [2] I. V. Andrianov, V. V. Danishevs'kyi, H. Topol, and D. Weichert. Homogenization of a 1d nonlinear dynamical problem for periodic composites. *ZAMM-Journal of Applied Mathematics and Mechanics/Zeitschrift für Angewandte Mathematik und Mechanik*, 91: 523–534, 2011.
- [3] I. V. Andrianov, V. V. Danishevs'kyi, O. I. Ryzhkov, and D. Weichert. Dynamic homogenization and wave propagation in a nonlinear 1d composite material. *Wave Motion*, 50: 271–281, 2012.
- [4] N. Bakhvalov and G. Panasenko. *Homogenisation: averaging processes in periodic media*. Mathematical problems in the mechanics of composite materials. Springer, 1989.
- [5] N. S. Bakhvalov and M. E. Eglit. Equations of higher order of accuracy describing the vibrations of thin plates. *J. Appl. Math. Mech. USSR*, 69:593–610, 2005.
- [6] T. Bennett and H. Askes. Finite element modelling of wave dispersion with dynamically consistent gradient elasticity. *Comput. Mech.*, 43:815–825, 2009.
- [7] T. Bennett, I. M. Gitman, and H. Askes. Elasticity theories with higher-order gradients of inertia and stiffness for the modelling of wave dispersion in laminates. *Int. J. Fract.*, 148:185–193, 2007.
- [8] A. Bensoussan, J. L. Lions, and G. Papanicolaou. *Asymptotic Analysis for Periodic Structures*. North-Holland, Amsterdam, 1978.
- [9] C. Boutin. Microstructural effects in elastic composites. *Int. J. Solids Struct.*, 33:1023–1051, 1996.
- [10] T. M. Chen. A modified hybrid laplace transform/finite element method for transient heat conduction problems. *Comput. Methods Appl. Mech. Engrg.*, 98:261–272, 1992.

- [11] W. Chen and J. Fish. A dispersive model for wave propagation in periodic heterogeneous media based on homogenization with multiple spatial and temporal scales. *ASME J. Appl. Mech.*, 68:153–161, 2001.
- [12] E. Cosserat and F. Cosserat. *Theorie des Corps Deformables*. Hermann & Fils, Paris, France, 1909.
- [13] J. A. Cottrell, T. J. R. Hughes, A. Reali, and G. Sangalli. Isogeometric discretizations in structural dynamics and wave propagation. In M. Papadrakakis, D. C. Charmpis, N. D. Lagaros, and Y. Tsompanakis, editors, *Proceedings of the ECCOMAS Thematic Conference on Computational Methods in Structural Dynamics and Earthquake Engineering*, Crete, Greece, June 13-16 2007.
- [14] E. V. Dontsov, R. D. Tokmashev, and B. B. Guzina. A physical perspective of the length scales in gradient elasticity through the prism of wave dispersion. *Int. J. Solids. Struct.*, 50:3674–3684, 2013.
- [15] J. Engelbrecht, A. Berezovski, F. Pastrone, and M. Braun. Waves in microstructured materials and dispersion. *Philos. Mag.*, 85:4127–4141, 2005.
- [16] C. Eringen and E. S. Suhubi. Nonlinear theory of micro-elastic solids II. *Int. J. Eng. Sci.*, 2:189–203, 1964.
- [17] J. Fish, W. Chen, and G. Nagai. Non-local dispersive model for wave propagation in heterogeneous media: multi-dimensional case. *Int. J. Numer. Meth. Engng.*, 54:347–363, 2002.
- [18] J. Fish, V. Filonova, and S. Kuznetsov. Micro-inertia effects in nonlinear heterogeneous media. *Int. J. Numer. Meth. Engng.*, 91:1406–1426, 2012.
- [19] S. Gonella, M. S. Greene, and W. Kam Liu. Characterization of heterogeneous solids via wave methods in computational microelasticity. *J. Mech. Phys. Solids*, 59:959–974, 2011.
- [20] S. M. Greene, S. Gonella, and W. K. Liu. Microelastic wave field signatures and their implications for microstructure identification. *International Journal of Solids and Structures*, 49:3148–3157, 2012.
- [21] J. M. Guedes and N. Kikuchi. Preprocessing and postprocessing for materials based on the homogenization method with adaptive finite element methods. *Comput. Meth. Appl. Mech. Engrg.*, 83:143–198, 1990.
- [22] T. Hui and C. Oskay. A nonlocal homogenization model for wave dispersion in dissipative composite materials. *Int. J. Solids Struct.*, 50(38-48), 2013.

- [23] W. J. Lee, J. W. Lee, and C. G. Kim. Characteristics of an electromagnetic wave absorbing composite structure with a conducting polymer electromagnetic bandgap (ebg) in the x-band. *Compos. Sci. Technol.*, 68:2485–2489, 2008.
- [24] K. A. Lurie. *An Introduction to the mathematical theory of dynamic materials*. Advances in Mechanics and Mathematics. Springer, 2007.
- [25] R. D. Mindlin. Micro-structure in linear elasticity. *Arch. Ration. Mech. Anal.*, 16:51–78, 1964.
- [26] S. A. Papanicolopoulos, A. Zervos, and I. Vardoulakis. A three-dimensional c^1 finite element for gradient elasticity. *Int. J. Numer. Meth. Engng.*, 77:1396–1415, 2009.
- [27] A. V. Porubov, E. L. Aero, and G. A. Maugin. Two approaches to study essentially nonlinear and dispersive properties of the internal structure of materials. *Phys. Rev. E*, 79(046608), 2009.
- [28] L. Ren and R. Zhang. Hybrid laplace transform finite element method for solving the convection–dispersion problem. *Adv. Water Resour.*, 23:229–237, 1999.
- [29] M. B. Rubin, P. Rosenau, and O. Gottlieb. Continuum model of dispersion caused by an inherent material characteristic length. *J. Appl. Phys.*, 77:4054–4063, 1995.
- [30] F. Santosa and W. W. Symes. A dispersive effective medium for wave propagation in periodic composites. *SIAM J. Appl. Math.*, 51:984–1005, 1991.
- [31] Z.-P. Wang and C. T. Sun. Modeling micro-inertia in heterogeneous materials under dynamic loading. *Wave Motion*, 36:473–485, 2002.
- [32] T. I. Zohdi. High-speed impact of electromagnetically sensitive fabric and induced projectile spin. *Comput. Mech.*, 46:399–415, 2010.
- [33] T. Suzuki and K. L. Zhang. Complex elastic wave band structures in three-dimensional periodic elastic media. *J. Mech. Phys. Solids*, 46:115–138, 1998.

$$\mathbf{A} \quad \langle \rho(\mathbf{y}) H_{ikl}(\mathbf{y}) \rangle = 0$$

Premultiplying Eq. 25 with the first order influence function, $\mathbf{H}(\mathbf{y})$ and integrating over the domain of the microstructure:

$$\int_{\Theta} H_{ikl} C_{ijpmn, y_j}^1 d\mathbf{y} = \int_{\Theta} \theta H_{ikl} D_{ipmn}^0 d\mathbf{y} - \int_{\Theta} H_{ikl} C_{ipmn}^0 d\mathbf{y} \quad (\text{A.1})$$

Integrating by parts leads to:

$$\int_{\Theta} H_{ikl} C_{ijpmn, y_j}^1 d\mathbf{y} = \int_{\Gamma} H_{ikl} C_{ijpmn}^1 n_j d\mathbf{y} - \int_{\Theta} H_{ikl, y_j} C_{ijpmn}^1 d\mathbf{y} \quad (\text{A.2})$$

The boundary integral vanishes due to periodicity. Considering Eq. 22 and 26, Eq. A.1 becomes:

$$\begin{aligned} & - \int_{\Theta} H_{ikl, y_j} C_{ijrs} (p_{rspmn} + H_{rmn} \delta_{sp}) d\mathbf{y} = \\ & \int_{\Theta} \theta H_{ikl} d\mathbf{y} D_{ipmn}^0 - \int_{\Theta} H_{ikl} C_{iprs} h_{rsmn} d\mathbf{y} - \int_{\Theta} H_{ikl} C_{iprs} \delta_{rm} \delta_{sn} d\mathbf{y} \end{aligned} \quad (\text{A.3})$$

Applying the averaging operator to the first term on the right hand side of the equation above:

$$\begin{aligned} & - \int_{\Theta} H_{ikl, y_j} C_{ijrs} p_{rspmn} - H_{ikl, y_j} C_{ijrp} H_{rmn} d\mathbf{y} = \\ & \frac{|\Theta|}{\rho_0} \langle \rho H_{ikl} \rangle D_{ipmn}^0 - \int_{\Theta} H_{ikl} C_{iprs} h_{rsmn} d\mathbf{y} - \int_{\Theta} H_{ikl} C_{ipmn} d\mathbf{y} \end{aligned} \quad (\text{A.4})$$

The major symmetry of \mathbf{C} suggests:

$$H_{ikl} C_{iprs} h_{rsmn} = h_{ijmn} C_{ijrp} H_{rkl} \quad (\text{A.5})$$

Define:

$$u_{klpmn} = \frac{1}{|\Theta|} \int_{\Theta} h_{ijkl} C_{ijrp} H_{rmn} d\mathbf{y} \quad (\text{A.6})$$

and $\hat{u}_{klpmn} = u_{klpmn} - u_{mnpkl}$, Eq. A.4 becomes:

$$- \int_{\Theta} h_{ijkl} C_{ijrs} p_{rspmn} d\mathbf{y} - |\Theta| \hat{u}_{klpmn} = \frac{|\Theta|}{\rho_0} \langle \rho H_{ikl} \rangle D_{ipmn}^0 - \int_{\Theta} H_{ikl} C_{ipmn} d\mathbf{y} \quad (\text{A.7})$$

Considering Eq. 18, premultiplying the equation with $\mathbf{P}(\mathbf{y})$ and integrating over the microstructure:

$$\int_{\Theta} P_{ipkl} C_{ijmn, y_j}^0 d\mathbf{y} = 0 \quad (\text{A.8})$$

Integrating by parts:

$$\int_{\Theta} P_{ipkl} C_{ijmn, y_j}^0 d\mathbf{y} = \int_{\Gamma} P_{ipkl} C_{ijmn}^0 n_j d\mathbf{y} - \int_{\Theta} P_{ipkl, y_j} C_{ijmn}^0 d\mathbf{y} \quad (\text{A.9})$$

The boundary integral vanishes due to periodicity and Eq. 22 yields:

$$\int_{\Theta} p_{ijpkl} C_{ijmn}^0 d\mathbf{y} = \int_{\Theta} p_{ijpkl} C_{ijst} h_{stmn} d\mathbf{y} + \int_{\Theta} p_{ijpkl} C_{ijst} \delta_{sm} \delta_{tn} d\mathbf{y} = 0 \quad (\text{A.10})$$

By virtue of the major symmetry of $\mathbf{C}(\mathbf{y})$,

$$\int_{\Theta} h_{ijkl} C_{ijrs} p_{rspmn} d\mathbf{y} = - \int_{\Theta} p_{rspmn} C_{rskl} d\mathbf{y} \quad (\text{A.11})$$

Using the above conclusion, Eq. A.7 becomes:

$$\int_{\Theta} p_{rspmn} C_{rskl} d\mathbf{y} - |\Theta| \hat{u}_{klpmn} = \frac{|\Theta|}{\rho_0} \langle \rho H_{ikl} \rangle D_{ipmn}^0 - \int_{\Theta} H_{ikl} C_{ipmn} d\mathbf{y} \quad (\text{A.12})$$

Integrating Eq. 26 over the microstructure:

$$\int_{\Theta} C_{klpmn}^1 d\mathbf{y} - \int_{\Theta} C_{klrp} H_{rmn} d\mathbf{y} = \int_{\Theta} p_{rspmn} C_{rskl} d\mathbf{y} \quad (\text{A.13})$$

Substituting Eq. A.13 into Eq. A.12:

$$\frac{|\Theta|}{\rho_0} \langle \rho H_{ikl} \rangle D_{ipmn}^0 = \int_{\Theta} C_{klpmn}^1 d\mathbf{y} - \int_{\Theta} H_{rmn} C_{rpkl} d\mathbf{y} - |\Theta| \hat{u}_{klpmn} + \int_{\Theta} H_{ikl} C_{ipmn} d\mathbf{y} \quad (\text{A.14})$$

Let:

$$v_{klpmn} = \frac{1}{|\Theta|} \int_{\Theta} H_{imn} C_{ipkl} d\mathbf{y} \quad (\text{A.15})$$

$$\hat{v}_{klpmn} = v_{klpmn} - v_{mnpkl} \quad (\text{A.16})$$

and defining \mathbf{D}^1 as:

$$D_{klpmn}^1 = \frac{1}{|\Theta|} \int_{\Theta} C_{klpmn}^1 d\mathbf{y} \quad (\text{A.17})$$

Eq. A.14 is written in terms of $\hat{\mathbf{w}}$ and \mathbf{D}^1 :

$$\langle \rho H_{ikl} \rangle D_{ipmn}^0 = \rho_0 (D_{klpmn}^1 - \hat{w}_{klpmn}) \quad (\text{A.18})$$

where:

$$\hat{w}_{klpmn} = \hat{u}_{klpmn} + \hat{v}_{klpmn} \quad (\text{A.19})$$

For macroscopically orthotropic materials, $\mathbf{D}^1 = 0$, then Eq. A.14 becomes:

$$\langle \rho H_{ikl} \rangle D_{ipmn}^0 = -\rho_0 \hat{w}_{klpmn} \quad (\text{A.20})$$

Noting that ρ_0 is independent of $\mathbf{H}(\mathbf{y})$, and that $\hat{\mathbf{w}}$ and \mathbf{D}^0 are independent of ρ , only the trivial solution is satisfied for an arbitrary chosen density variation within the microstructure:

$$\langle \rho H_{ikl} \rangle = 0 \quad (\text{A.21})$$

B Moore - Penrose pseudo-inverse

The Moore-Penrose pseudo-inverse $\mathbf{A}^{-\text{mp}}$ of a matrix \mathbf{A} is a generalization of the inverse matrix. Let \mathbb{K} denote one of the fields of real or complex numbers, $M(m, n; \mathbb{K})$ denote the vector space of $m \times n$ matrices over \mathbb{K} . For $\mathbf{A} \in M(m, n; \mathbb{K})$, a Moore-Penrose pseudo-inverse of \mathbf{A} is defined as a matrix $\mathbf{A}^{-\text{mp}} \in M(n, m; \mathbb{K})$ satisfying all of the following four criteria:

$$\mathbf{A} \mathbf{A}^{-\text{mp}} \mathbf{A} = \mathbf{A} \quad (\text{B.1})$$

$$\mathbf{A}^{-\text{mp}} \mathbf{A} \mathbf{A}^{-\text{mp}} = \mathbf{A}^{-\text{mp}} \quad (\text{B.2})$$

$$(\mathbf{A} \mathbf{A}^{-\text{mp}})^* = \mathbf{A} \mathbf{A}^{-\text{mp}} \quad (\text{B.3})$$

$$(\mathbf{A}^{-\text{mp}} \mathbf{A})^* = \mathbf{A}^{-\text{mp}} \mathbf{A} \quad (\text{B.4})$$

where the superscript $*$ denotes the Hermitian transpose. Moore - Penrose pseudo-inverse exists and is unique. Equations B.1 and B.2 define the generalized inverse and Eqs. B.3 and B.4 determine the uniqueness of the pseudo-inverse of \mathbf{A} .